UNIVERSITY OF BERGEN

GEOPHYSICAL INSTITUTE

Master Thesis in Energy

Specialization in Energy Technology

Electrical Power engineering

Frequency Regulation of Synchronous Generator

By: Stian Jensen Sørås

June 1, 2017

Abstract

The objective of this thesis is to create a Load Frequency Control (LFC) to regulate the active power output and frequency of a synchronous generator, and to conduct experiments to verify frequency stability.

The electrical parameters of the synchronous generator will be determined through testing. The dynamic response of the prime mover and generator will be found experimentally by evaluating the step response. A Proportional-Integral-Derivative Controller (PID) will be tuned with various techniques, then implemented on a loaded generator. A change in loading will be applied to the generator, and the controller will attempt to maintain the synchronous speed.

The electrical parameters of the generator were verified through multiple tests. It is shown that the Variable Frequency Drive (VFD) PID that controls the prime mover managed to maintain close to synchronous speed when a change in load occurred, within required tolerance. The mechanical constants of the generator and prime mover has been calculated by evaluating the dynamic response and measured mechanical torque, and is consistent with parameters from machine data sheets. A stability analysis has been performed on the controller loop, indicating stability around the working point.

Acknowledgement

This Electric Power engineering master thesis mark the end of my six year run at Western Norway University of Applied Sciences.

I wish to express my sincere gratitude towards my supervisor, Associate Professor Emil Cimpan; for helpful advise, inspiring guidance and that extra interest in control systems. A big thanks to Senior Engineer Lars Manger Ekroll, for his ability to solve everything.

I wish to thank my fellow students Ole-Jan Aarhuus Amundsen and Sven Arild Kjerpeset for making these two years as a master student fly away. A special thanks to Lars Eirik Eilifsen, for teaching me the finer points of Latex and Matlab, and for our good collaboration in the lab. A special thanks to Terje Jensen Sørås, for reviewing this text, and making appropriate suggestions/corrections when I was becoming gradually more word-blind.

This being the end of my carrier as a student, I would sincerely thank Bergen Teknikersamfund and Kronbar for the important job these organizations do for every student at this campus.

Bergen, 2017

Stian Jensen Sørås

Table of Contents

1 Introduction **1**

1.1 Background 1
1.2 Literature Review 3
1.3 Object of Thesis 5
1.4 Method 6
1.5 Structure of Thesis 7

2 Synchronous Machine Theory **9**

2.1 Equivalent Circuit 10
2.2 Circuit Model 13
2.3 Park's Transform 15
2.4 The Mechanical System of a Synchronous Machine 18
2.5 Generator Voltage Control 21
2.5.1 Excitation Systems 22
2.6 Load Frequency Control 22
2.6.1 Area Control Strategies 24

3 Machine Test Procedures and Parameter Determination **27**

3.1 Open Circuit Test 27
3.2 Sustained Short-Circuit Test 29
3.3 Slip Test 31
3.4 Armature Leakage Reactance of the Stator 32
3.4.1 Potier-method 32
3.5 Signal Conditioning 34
3.5.1 Signal Filtering 34
3.5.2 Uncertainty in Measurements 35

4 Generator Control System **37**

4.1 Transient Response, Steady-State and Stability 37
4.1.1 Stability of a Control System 38
4.2 Second-Order Systems 39
4.3 PID Controller 41
4.3.1 Proportional 41
4.3.2 Integral 42
4.3.3 Derivative 42

5 Method **43**

5.1 Prime Mover 43

5.1.1 DC Machine 44
5.1.2 Induction Machine 45
5.2 Open-circuit and Short-Circuit Characteristics 46
5.3 Potier Reactance test 47
5.3.1 Zero Power Factor Characteristics 47
5.3.2 Potier Triangle 48
5.4 Slip Test 49
5.5 Prime Mover Experimental Step Response 49
5.5.1 PID Controller Tuning 50
5.5.2 Prime Mover with PID Controller 52
5.6 Prime Mover and Generator with a Resistive Load 53
5.6.1 Construction of the Transfer Function 53
5.6.2 PID Tuning 54
5.6.3 Dynamic Response with Change in Resistive Load 55
5.6.4 Stability Analysis with Root Locus 55
5.7 Mechanical Machine Constants 56
5.8 Measurement in a Laboratory Environment 57
5.8.1 Noise Reduction 57
5.8.2 Filtering and Sample Rate 57

6 Result **59**
6.1 Open-Circuit and Short-Circuit Characteristics 59
6.2 Potier Reactance 62
6.3 Slip Test 64
6.4 Prime Mover Experimental Step Response 66
6.4.1 Prime Mover with PID Controller 67
6.5 Prime Mover and Generator with a Resistive Load 71
6.5.1 PID Tuning 72
6.5.2 Dynamic Response with Change in Resistive Load 76
6.5.3 Stability Analysis with Root Locus 78
6.6 Mechanical Machine Constants 82
6.6.1 No Load Machine Constants 82
6.6.2 Moment of Inertia With Rated Load 83
6.7 Measurement in a Laboratory Environment 86
6.7.1 Uncertainty in Measurements 86
6.7.2 Noise Reduction 87
6.7.3 Periodic Noise in Measurements 87

7 Discussion **89**

8 Conclusion **91**

References **93**

A Laboratory Instruments **96**

B DC Machines **96**

C Induction Machines **98**

List of Figures

2.1 Cylindrical rotor and salient pole rotor design 11
2.2 Phasor diagram for the two-reaction model 12
2.3 Classification of power system stability 19
2.4 IEEE basic blockdiagram of an excitation system 21
3.1 Open-circuit characteristics of a synchronous machine 29
3.2 Open- and short-circuit curve characteristics 31
3.3 Determination of the Potier-reactance 33
4.1 Step Response for Second-Order Systems with different damping . . 40
5.1 Circuit diagram of circuit to deliver step to the PWM 44
5.2 Circuit diagram of circuit to deliver step to VFD 45
5.3 Proposed blockdiagram for prime mover with PID control 53
5.4 Blockdiagram for the system with controller and feedback loop 54
6.1 Open-Circuit and Short-Circuit Characteristics for Terco MV1027-235 Synchronous generator, using method 1. 61
6.2 Open-Circuit and Short-Circuit Characteristics for Terco MV1027-235 Synchronous generator, using method 2. 62
6.3 Plot showing the OCC and ZPFC curves, the Potier triangle is plotted with the dotted line. 63
6.4 Enhanced picture of the Potier triangle. 64
6.5 4 % Slip Test, armature voltage and armature current plotted against each other. 65
6.6 4 % Slip Test, plot of field voltage, armature voltage and armature current. 65
6.7 The dynamic response of the prime mover 68
6.8 The Bode plot of the frequency response 68
6.9 Prime Mover with Ziegler-Nichols PID 69
6.10 Prime Mover with Pole-Zero cancellation PID 69
6.11 Prime Mover with Cohen-Coon PID 70
6.12 Prime Mover with Frequency Response PID 70
6.13 The derivative of the system response. 72
6.14 Reaction curve for a loaded generator 73
6.15 The first order approximation of the response 74
6.16 Bode Plot used to tune the PID regulator 75
6.17 PID response when given an increment in load 77
6.18 Enhanced picture of PID response in Figure 6.17 77
6.19 Dynamic response of loaded generator with Cohen-Coon tuned PID 78

6.20 Root Locus of the closed-loop system 79
6.21 Root Locus of the Cohen-Coon PID Controller 80
6.22 Dynamic response of closed loop system with controller gain 0.1 . . . 81
6.23 Dynamic response of closed loop system with controller gain 12.9 . . 81
6.24 Speed Plot unloaded generator 83
6.25 Torque Plot for unloaded generator and prime mover 84
6.26 Torque Plot Generator with 1050W Active Load 84
6.27 Effects of noise reduction on a step response 87
6.28 Periodic disturbance in measurements 88
B.1 Crossection of a dc machine 97
C.1 A typical graph of the motor speed-torque characteristic for asynchronous machine 99

List of Tables

1 Reactances in the synchronous machine 13
2 Synchronous machine nameplate 43
3 DC machine nameplate 45
4 Induction machine nameplate 46
5 Ziegler-Nichols tuning with reaction curve 51
6 Cohen-Coon tuning with the reaction curve 52
7 Bode Plot Tuning parameters used for PID-regulators. 52
8 Experimental working points for dynamic response 53
9 Base values for Terco MV1027-235 Synchronous Generator 59
10 Experimental data recorded during Open-Circuit and Sustained Short-Circuit test. 60
11 PID Tuning parameters for the prime mover 67
12 Experimental time constants 72
13 PID Tuning parameters for the loaded generator, calculated. 75
14 PID Tuning parameters for loaded generator, experimental. 76
15 Accuracy of laboratory instruments 86
16 Instruments and devices 96

Abbreviations

AC Alternating Current. 2

AFNL Amperes Field No Load. 30

AFSC Amperes Field Short Circuit. 30

AGC Automatic Generation Control. 4, 5, 23–25, 37

AVR Automatic Voltage Regulator. 21, 22, 90

CIGRE Conseil International des Grands Réseaux Électriques. 4, 19

DC Direct Current. 2, 89

DTC Direct Torque Control. 76, 82, 89

emf electro-motive force. 11, 13, 15, 20, 28

EU European Union. 3

EWH Electrotechnische Werkstätten Hof. 47

GUM Guide to the expression of uncertainty in measurements. 35

IEEE Institute of Electrical and Electronics Engineers. 4, 19

LFC Load Frequency Control. iii, 1–3, 5, 23, 25, 89, 90, 92

mmf magneto-motive force. 27, 31

NPS Nord Pool Spot. 3, 25

OCC Open-Circuit Characteristic. 27, 32, 34, 43, 44, 46–48, 57, 59, 61, 62, 90

PF Power Factor. 2, 9

PID Proportional-Integral-Derivative Controller. iii, 5, 41, 45, 50, 54, 55, 59, 71, 76, 79, 80, 82, 89, 91

PSS Power System Stabilizer. 21

RMS Root-Mean-Square. 11, 58

SCR Short-Circuit Ratio. 30

SSC Sustained Short-Circuit. 29, 32, 43, 44, 46–48, 57, 59, 61, 90

TF Transfer Function. 38, 39, 41, 52, 54, 55, 67, 74, 78

VFD Variable Frequency Drive. iii, 45, 50, 52, 53, 57, 67, 71, 76, 82, 88–92, 96

ZPFC Zero Power Factor Characteristic. 32, 47, 48, 62

1 Introduction

Ensuring stability, reliability and security in power systems is of paramount importance to system operators and the end-user [1]. Load Frequency Control (LFC) is a term used to describe the control of power output and frequency of the generating units [2, pp. 582]. To regulate the power output, the operator must increase or decrease the mechanical input with respect to the time-changing load in order to keep power balance in the interconnected system. The goal of LFC is to supply the desired active power while maintaining the system frequency. For the Nordic power grid, the system frequency is required to stay within the tolerance 49.9 to 50.1 Hz. If the frequency deviates from this an increment in power generation is required. Statnett is responsible for monitoring the frequency in Norway, and facilitating the correct adjustments in power generation [3]. The EN50160 standard sets the limit to ± 1% of rated frequency as the absolute limit [4]. An interconnected power system is a vast leviathan; dynamic and ever-changing. As stated by C. Steinmetz; *the North American interconnected power system is the largest and most complex machine ever devised by man* [2, pp. xix]. Albeit smaller, this statement also stands true for the international power system we have in Scandinavia and North-Europe.

1.1 Background

Electricity, and especially lightning, is a phenomenon that has always stunned and intrigued mankind. The Egyptians first noticed that an invisible charge of power would appear when a piece of raven was rubbed against a piece of cloth. The works of Benjamin Franklin and his peers gave a fundamental understanding of electrical phenomena, describing electricity as a subtle substance to which a matter, or conductor, was needed to direct its charge. Franklin was one of the first scientists to develop the theory of electrons, small charges moving between atoms [5]. During the 19th century, European scientists created the theory of electric and magnetic forces, and Maxwell connected all these phenomenas together with a set of beautiful equations, which built the foundation for calculating magnetic and electric fields and all electromagnetic phenomena. Towards the turn of the century, Thomas Alva Edison developed the first publicly available power system in New

York, operating at 110 V Direct Current (DC). At GE Electric, the Croatian engineer Nikola Tesla worked on improving Edison's system. Tesla experimented with Alternating Current (AC) current, a field that Edison did not share Tesla's enthusiasm for [6, pp. 1057]. Later, Nicola Tesla quit his job at GE Electric, and further developed the theory that led to the first three-phase AC power system. The new system lifted the constraints on transmission distance that troubled Edison's power network. In his works with AC, Tesla also invented several new machines. One machine was *a form having a comparatively small rotary effort at start but maintaining a perfect uniform speed, which motor has been termed synchronous.* The other version provided *a great rotary effort at start, the speed being dependent on the load.* With these sentences Tesla describes the synchronous machine and induction machine in the same paper [7].

At first, most power system operated individually. At the turn of the 18th century, this meant the dozen blocks that could be reached from the 110 V power line from the Edison Bipolar in New York. Clearly, this meant an ineffective power transmission, with huge losses and instability. During the 1920's and 1930's, utility suppliers in America started imagining a completely electrified country, the idea had its root in the southeastern states. Supply and demand was the initial idea; a station with a surplus production could sell this energy to a station that lacked energy to supply its load. To achieve this goal, the utility suppliers faced several obstacles. They had to collaboration on load planning in order to evaluate the balance of hydroelectric and steam power generation. At power plants, synchronous condensers were commissioned to improve the Power Factor (PF); an attempt to operate all power plants at a unify PF. To ensure system stability when running parallel tie-lines, it was early recognized that the system frequency had to be kept firmly at 60 Hz. The Load Dispatchers had the authority to act and adjust power generation in order to keep the entire interconnected power system up and running [8, pp. 1238]. The basic idea of LFC is very much the same today.

In Scandinavia, the interconnected power system includes Norway, Sweden, Denmark, Finland, Estonia and Lithuania. Several tie-lines to Great Britain and Europe are also under construction. In the interconnected Scandinavian system the goal is to create a liquid and transparent power marked, where free competition forces

the prices towards a social optimum, and removes the possibility of participants enforcing marked power. Thus, the prices are kept low and are extremely volatile [9]. Nord Pool Spot (NPS) was the first international power exchange in the world, and is an example on how marked integration can lead to a stable and efficient marked. In order for this to work, LFC must be applied to regulate the frequency, and to control the power balance. An agreement between the participating parties regulate every aspect of the interconnected transmission, from load shedding, frequency control and voltage control [3].

European Union (EU) introduced several environmental requirements for all member countries, which leads to what Norway has called the *green shift*. These requirements effectively forces the societies towards new, renewable energy sources. NPS is affected by this, as the basic thermal power generation units, such as coal-fired steam plants and nuclear plants are replaced with volatile energy sources such as wind- or solar energy. Proper control of voltage levels, frequency, and reduction of harmonics are criteria for supplying electric energy of good quality [10, pp. 16]. Reduction in thermal generating units across Europe and Scandinavia means that the bulk of power supplied will have to come from hydroelectric plants, and that their operation are paramount in regulating the frequency.

Great pressure is applied on the utility suppliers, as they have to meet the public's demand for electrical energy while avoiding to make a harmful impact on the environment. Environmental issues are ever-present on the political agenda, and commissioning of new power plants is very difficult because of the wish for a sustainable future. Power plants have always been a major source of pollution, and it is estimated that power generation is responsible for one third of the world's CO_2 emission [10, pp. 16].

1.2 Literature Review

LFC of the synchronous generator is an important and mature subject, in which many studies have been conducted. The fundamentals of the synchronous machine has changed little since the beginning of the 20th century. Countless books and articles have been written on every subject regarding the synchronous ma-

chine, excitation and governor systems, dynamics and stability, by important organizations such as Conseil International des Grands Réseaux Électriques (CIGRE) and Institute of Electrical and Electronics Engineers (IEEE). The author have used articles on test procedures and generator modeling as well as several other articles to compile the theory chapter in this thesis [1, 11–13]. The articles from IEEE are descriptive, and thoroughly reviewed by a large scientific body.

To derive the basic theory of the synchronous machine the author have used the excellent books by S. Umans [14] and Bergen and Vittal [15]. A good supplement to these books is the descriptive book by J. Machowski, J. Bialek and J. Bumby [10], who's content contain a careful review of machine fundamentals, basic circuitry and advanced power system dynamics. The textbook written by P. Kundur [2] is referred to in numerous articles, and is a well-renowned tool for electrical engineers working with power system stability.

The fundamentals of interconnected systems are the same, although power systems have undergone a huge technological development in the 20th century. The basic difficulties of connecting several systems together still remain, and have been covered in the excellent paper by W. E Mitchell [8]. This article also give a fascinating image of the early days of the power system integration in America. In [16] the principles of Automatic Generation Control (AGC) is covered skillfully and neutrally, as there are various setups available for the system operator to choose from. Power system stability is covered in most of the previously mentioned textbooks, and in an article by Kundur et. al [1].

Performance characteristics of machines are found by subjecting the machine to a set of tests. Such tests are covered in papers throughout the development of the synchronous machine theory [17–19], and the procedures are standardized in IEEE Std.115 [11].

Control systems are covered in multiple books and papers. The groundbreaking article by Ziegler and Nichols set the frame for parameter tuning in control systems [20]. N. Nise [21] have written an extensive textbook on control systems, which has been a great asset in the work during this thesis.

1.3 Object of Thesis

The objective of this thesis is to create a LFC to regulate the active power output and frequency of a synchronous generator in the event of a disturbance or change in load.

The electrical parameters of the synchronous generator will be found experimentally through tests. These characteristics will be used to create a model of the synchronous machine, that can be used in an AGC model.

Attention is then turned to the mechanical prime mover, which will be represented by: (i) a dc machine; and (ii) an induction machine. An approximation of the dynamic response during a step will be developed to model the prime mover action. The study will then extend to the tuning and experimental testing of different control systems for the prime mover. The response of controller tunings will be examined experimentally.

Further, the initial prime mover model will then be combined with the synchronous generator model. The dynamic response will be obtained by applying a step in speed, and an approximation will be developed from the response. A Proportional-Integral-Derivative Controller (PID) controller will be designed to regulate the speed of the system. This controller completes the LFC loop. A change in load will be applied to the synchronous generator to examine if the controllers maintains synchronous speed. The frequency must be in compliance with local rules and regulations [3]. The study will yield the mechanical machine constants for a combined system, which can be used to model the mechanical system in an AGC system.

A stability analysis will also be performed on the closed loop system using the dynamic model of the generator and power control system. Stability boundaries will be located and simulated in Matlab.

1.4 Method

The author will have a qualitative approach to the objective of this thesis, the objective will be solved experimentally. Data collected through experiments will then be processed in Matlab or by hand calculations.

The first step is to acquire the generator parameters, in an attempt to verify the new generator. Data is recorded with a combination of conventional voltage meters, Fluke Power Quality Analyzer, and a Picometer Digital Oscilloscope. Matlab computer software is then used to process the signals, and to develop graphics and mathematical solutions.

Next, the testing will commence on the prime mover. A step will be applied to the controller box of the prime mover, initiating an acceleration in speed. The dynamic response of the prime mover is obtained, and processed into a dynamic model. A PID controller will then be calculated using several different tuning rules. The controller will be implemented, and the system response will be examined.

The synchronous generator and an active load will be connected. A step will be applied, and the response of the combined system will be checked for several different load values. At nominal rating, a measurement will be taken and processed into an approximation of the system response. A controller will be designed to suit the approximation. The system will be placed under controller regulation, and a step will be applied in the active load.

The mechanical machine constants of the synchronous machine and prime mover will be derived from the measurements, by examining the mechanical torque, speed, electrical torque and acceleration time.

A stability analysis will be performed using the Root Locus technique. This will be used to find the critical gain(s) for keeping stability in the combined system.

1.5 Structure of Thesis

The thesis is structured as following: Section 2 cover the synchronous machine theory, its equations, and the ingenious Park's transform. An short summary of power system stability is included, that delves into the mechanical equations, and their importance on stability. Section 3 cover the various tests that is applied to the synchronous machine in order to determine its parameters. A brief introduction to signal conditioning is also presented. Section 4 deals with the important subject of control system engineering, stability and dynamic response. Dynamic controllers is also introduced. Section 5 presents the method applied in order to solve the objective of the thesis. Section 6 details the results of the thesis. Section 7 will then present a discussion of the results. Future work is described. Section 8 contains the conclusion.

2 Synchronous Machine Theory

The synchronous generator is the most common machine used to feed electrical energy into our power systems. The synchronous machine is also used as an electric motor, especially in applications which require a steady, reliable speed. But, the synchronous machine used as generator far excels its use as a motor. High reliability and cost-effectiveness makes this machine outstanding for producing a steady supply of electrical energy. The synchronous generator can be used in combination with all kinds of mechanical systems: (i) steam-driven turbines; and (ii) hydro-driven turbines.

The synchronous machine has a rotating speed that is closely related to the frequency in the grid. This gives the machine high resilience towards changes in voltage. In synchronous machines the PF, reactive power and terminal voltage is controlled by adjusting the field current supplied by the exciter. By adjusting the mechanical input, affecting the rotational speed of the turbine, the electrical frequency and active power of the generator can be regulated. Equation (2.1) show the relationship between the number of poles of the machine, the generator speed in rpm and the electric frequency.

$$f_e = \left(\frac{p}{2}\right)\frac{n}{60}\,[Hz] \tag{2.1}$$

Where f_e is the electrical frequency, p is the number of poles for the machine, and n is the rated speed of the machine.

The induced voltage in the generator is found by evaluating the magnetic field, and the interaction between the windings in the machine and the field. Equation (2.2) show how the induced voltage is deducted from the time-derivative of the flux linkages linking coil a, with generator notation.

$$e_a = -\frac{d\lambda_a}{dt} + r\,i_a \tag{2.2}$$

where λ_a is the instantaneous value of flux linkage, t is the time, r is the resistance of the stator winding, and i_a is the current flowing through the stator winding. With the latter part added, Equation (2.2) show the terminal voltage of phase a.

The synchronous machine can be approached from two different viewpoints; (i) the machine viewpoint, or (ii) the circuit viewpoint [14, 15]. For steady-state, positive sequence operation, the machine viewpoint yields a perfectly acceptable result. The model is constructed by considering the rotating fields in the machine. Basic voltage-generation mechanisms is clearly described, and the model can be used to analyze electro-mechanical transients. The machine viewpoint is derived in Section 2.1.

When considering transients, such as short-circuit on generator terminals or negative sequence operation, the steady-state model can not be applied. The circuit viewpoint is used when a more accurate model is needed. The circuit elements, and their dependence on rotor position, is taken into the model. In Section 2.2 the matrix for this model is shown. Often, the circuit model can yield difficult equations, so the Parks transform is introduced in Section 2.3 to simplify these [15]. The result of this transform is a much more simple, constant and sparse matrix.

The synchronous generator has two inputs: (i) field voltage and (ii) mechanical input. These inputs regulate the induced voltage and the electrical frequency of the current. These systems are named the electric system and the mechanical system, and both have to be modeled in order to create a complete dynamic model of the generator.

2.1 Equivalent Circuit

The terminal voltage of a synchronous machine is determined by evaluating the *open circuit voltage* and the *armature reaction*.

The open-circuit voltage is the voltage that is induced in the machine due to the magnetic field in the field winding alone, i.e $i_a = i_b = i_c = 0$. The armature reaction is a voltage that is induced by the currents flowing in the stator circuit, with the field current $i_F = 0$ [15, pp. 190–191]. It is important to notice that the armature voltage is working against the open-circuit voltage, limiting the terminal voltage. If not, the more current the load is consuming, the more energy the generator would deliver, i.e a perpetual motion machine. The terminal voltage is found by taking

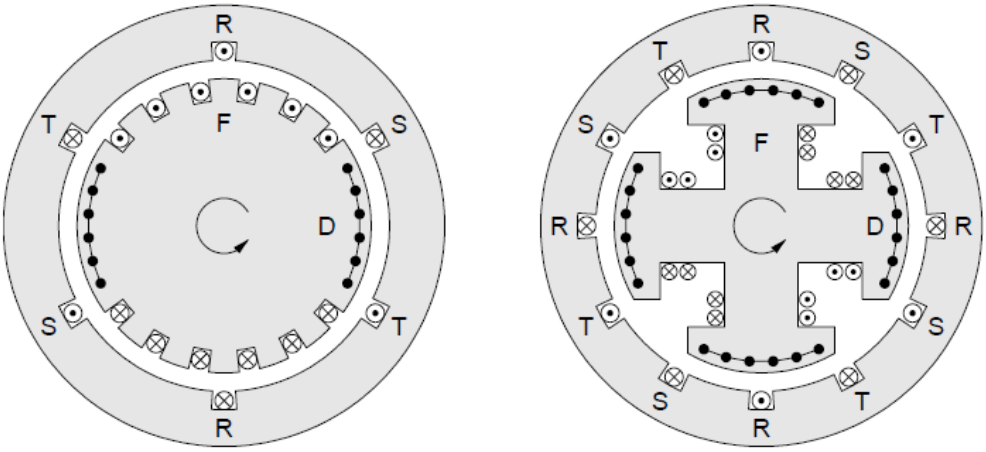

Figure 2.1: Cylindrical rotor and salient pole rotor design. Notice that the round rotor is a two-pole winding with dampers, while the salient type has 4 poles. The damper windings can be spotted on the protruded poles.

the superposition of the open-circuit voltage and armature reaction, and adding them up [15, pp. 196].

The terminal voltage, in the machine viewpoint and time domain, can then be expressed as

$$v_a = R_a i_a + L_s \frac{d i_a}{d t} + e_{af} \tag{2.3}$$

This equation is expressed in Root-Mean-Square (RMS) complex magnitudes. e_{af} is the generated voltage, induced by the field winding flux. It is also called the *internal voltage* [14, pp. 269]. Equation (2.4) is the basic equation in phasor form for determining the induced voltage in a synchronous machine with round rotor.

$$E_a = V_a + I_a(r + jX_s) \tag{2.4}$$

where E_a is the induced electro-motive force (emf) of the machine, V_a is the terminal voltage, I_a is stator current, r is resistance in the winding of the machine and X_s is the synchronous reactance.

For the round rotor, the air-gap between the rotor and stator is uniform, and very small. This is not the case when we have a salient pole type machine. As shown in

Figure 2.1, the air-gap is larger in the quadrature axis, perpendicular to the pole axis. Since the air gap is much larger in the quadrature direction, the current i_a is less effective in producing the flux. As a result we get a smaller inductance parameter [15, pp. 199].

Thus, it is necessary to develop a model using direct- and quadrature axis parameters, called *two-reaction model* [15, pp.201]. The two-reaction model was developed by Park, and was a refinement of the previous work by Blondel, Dreyfus, Nickle and Dorothy [22, 23].

The two-reaction model relies heavily on the Park's transform, especially for transient and unsymmetrical load conditions. Most parameters for synchronous generators will be given as direct- and quadrature axis quantities.

$$I_{aa} = I_{ad} + I_{aq} \tag{2.5}$$

The axes of the two-reaction model are perpendicular on each other, the same relates the currents flowing in the direct and quadrature axis. Figure 2.2 show the phasor diagram for this situation. The terminal voltage lies along the same axis as the quadrature component, and the direct axis is phase-shifted ∠90. The syn-

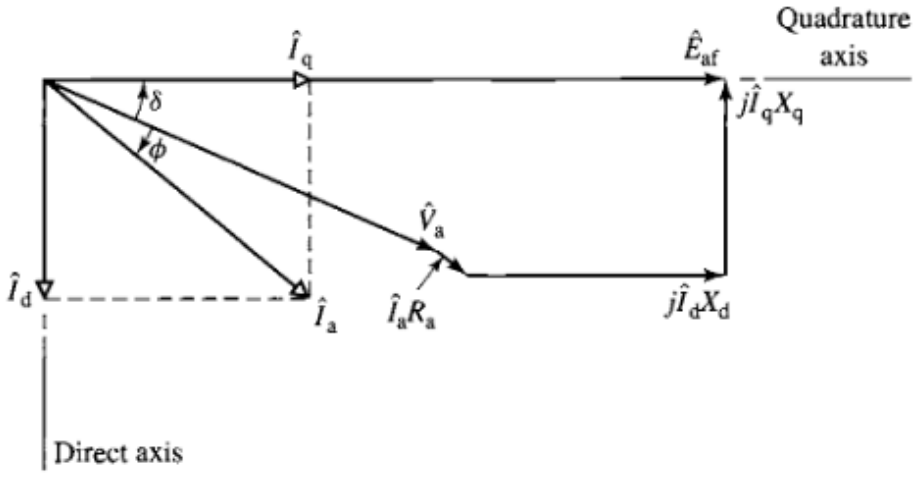

Figure 2.2: Phasor diagram for the two-reaction model. Adapted from[14]. Notice that the notation for the phasors (e.g. $\hat{I}_a$) in the figure differs from what the author has used in this thesis.

chronous reactance X_s will in this case be resolved into the direct axis reactance

X_d and the quadrature axis reactance X_q. Equation (2.6) is the equation for determining the voltages in a salient pole synchronous machine.

$$E_a = V_a + r\,I_a + I_d\,j\,X_d + I_q\,j\,X_q \tag{2.6}$$

where E_a is the induced emf of the machine, V_a is the terminal voltage, r_a is the resistance in the windings, I_d is the current in the direct axis, X_d is the direct axis reactance, I_q is the current in the quadrature axis, X_q is the quadrature axis reactance.

Park and Robertson [19] have summed opp the different reactances of interest in a salient synchronous generator. If there are no windings on the quadrature axis,

Table 1: Reactances in the synchronous machine

Notation	Name
X_d	Direct axis synchronous, positive phase-sequence
X_q	Quadrature axis synchronous, positive phase-sequence
X'_d	Direct axis transient, positive phase-sequence
X'_q	Quadrature axis Transient, positive phase-sequence
X''_d	Direct axis sub-transient, positive phase-sequence
X''_q	Quadrature axis sub-transient, positive phase-sequence
X_2	Negative phase-sequence
X_0	Zero phase-sequence

the following relation exists.

$$X''_q = X'_q = X_q \tag{2.7}$$

If there are damper windings on the quadrature axis, the sub-transient will differ from the transient and quadrature reactance. Because the quadrature axis do not have any effective windings, X_q=X'_q is still a valid assumption [19, pp. 518].

2.2 Circuit Model

In this section, the synchronous generator is presented from the circuit viewpoint. This model is general and more appropriate to use when considering transients

from short-circuits and unbalanced operation [15, pp. 215]. It is desirable to derive an equivalent circuit of the machine based on steady-state characteristics.

Before the machine inductances is derived, the circuit matrix for stator and rotor variables in the synchronous machine is defined. The circuit consists of three phase-windings on the stator, a field winding and two (or more) fictitious windings located on the rotor that model the short-circuited path of the damper windings [15].

$$\begin{bmatrix} v_{a'a} \\ v_{b'b} \\ v_{c'c} \\ v_{FF'} \\ v_{DD'} \\ v_{QQ'} \end{bmatrix} = \begin{bmatrix} r & & & & & \\ & r & & & & \\ & & r & & & \\ & & & r_F & & \\ & & & & r_D & \\ & & & & & r_Q \end{bmatrix} \begin{bmatrix} i_a \\ i_b \\ i_c \\ i_F \\ i_D \\ i_Q \end{bmatrix} + \frac{d}{dt} \begin{bmatrix} \lambda_{aa'} \\ \lambda_{bb'} \\ \lambda_{cc'} \\ \lambda_{FF'} \\ \lambda_{DD'} \\ \lambda_{QQ'} \end{bmatrix} = \mathbf{Ri} + \frac{d\lambda}{dt} \tag{2.8}$$

Where lower case letters indicate stator variables, and upper case describes rotor variables. The vector **R**=diag(r,r,r,r_F,r_D,r_Q) describes the resistance r of each phase winding, r_F describe the resistance of the field winding, r_D and r_Q describes the resistances of the direct axis and quadrature axis damper windings.

Equation (2.8) can be expressed in vector form, as shown in the latter half of the equation. This equation takes the circuit viewpoint, in the following analysis it is necessary to use the generator viewpoint. A voltage vector is defined, which deal with the subscripts in Equation (2.8) [15]:

$$\mathbf{v} \triangleq \begin{bmatrix} v_a \\ v_b \\ v_c \\ -v_F \\ -v_D \\ -v_Q \end{bmatrix} \tag{2.9}$$

Using Equation (2.9) in Equation (2.8), the vector now is:

$$\mathbf{v} = -\mathbf{Ri} - \frac{d}{dt}\lambda \tag{2.10}$$

Equation (2.10) is called the *the electrical equation*. Using the generator viewpoint it derives the terminal voltage based on the induced emf in the machine and the voltage drop in the winding resistances. The next step is to derive an expression for the electric torque in the machine.

$$J\ddot{\theta} + D\dot{\theta} - \frac{1}{2}\mathbf{i}^T \frac{d\mathbf{L}(\theta)}{d\theta}\mathbf{i} = T_m \Longleftrightarrow J\ddot{\theta} + D\dot{\theta} + i_q\lambda_q - i_d\lambda_d = T_m \tag{2.11}$$

where J is the moment of inertia of the synchronous machine, and D is the damping of the machine. T_m is the *mechanical torque*. The latter half of the equation can either be expressed in terms of currents and inductances, or by Parks variables seen on the equation to the right. Equation (2.11) is called *the mechanical equation*. In the mechanical equation it is noticed that direct axis and quadrature axis parameters are used, which requires an introduction to the Park's transform.

2.3 Park's Transform

The Parks transform is a technique where stator parameters are expressed as rotor parameters. In the circuit analysis the parameters are given as stator quantities, and the inductance is observed as time-varying by the stator phase, due to the rotation of the field winding. When the stator parameters are transformed to rotor quantities, the variables rotate with the rotor, and experience constant magnetic paths [14, pp. 664]. All inductances in the Park's transform are independent of rotor angle, and are constant and independent of time [10, pp. 438].

The transform was derived by A. Blondel in France. R. E. Doherty, C. A. Nickle and R.H Park further developed the transform. It is therefore known as either Park, Blondel or 0dq-transform [14, pp. 665]. The transform is applicable on stator currents, voltages and flux linkages. In many cases the transform yields simpler equation, and for some special cases the transform yields a linear time-invariant equation.

All windings in the generator are magnetically coupled, giving that the flux in each winding is dependent on the current in the other windings [10, pp. 434]. Equation

(2.12) shows how each of the generator windings are coupled.

$$\begin{bmatrix} \lambda_a \\ \lambda_b \\ \lambda_c \\ \lambda_F \\ \lambda_D \\ \lambda_Q \end{bmatrix} = \begin{bmatrix} L_{aa} & L_{ab} & L_{ac} & L_{aF} & L_{aD} & L_{aQ} \\ L_{ba} & L_{bb} & L_{bc} & L_{bF} & L_{bD} & L_{bQ} \\ L_{ca} & L_{cb} & L_{cc} & L_{cF} & L_{cD} & L_{cQ} \\ L_{Fa} & L_{Fb} & L_{Fc} & L_{FF} & L_{FD} & L_{FQ} \\ L_{Da} & L_{Db} & L_{Dc} & L_{DF} & L_{DD} & L_{DQ} \\ L_{Qa} & L_{Qb} & L_{Qc} & L_{QF} & L_{QD} & L_{QQ} \end{bmatrix} \begin{bmatrix} i_a \\ i_b \\ i_c \\ i_F \\ i_D \\ i_Q \end{bmatrix} \tag{2.12}$$

Small caption refers to stator quantities, while a big caption is used for rotor parameters. By using Equation (2.13) the stator parameters are transformed to rotor quantities, avoiding the variations caused by the rotation of the rotor.

$$\begin{bmatrix} i_0 \\ i_d \\ i_q \end{bmatrix} = \sqrt{\frac{2}{3}} \begin{bmatrix} \frac{1}{\sqrt{2}} & \frac{1}{\sqrt{2}} & \frac{1}{\sqrt{2}} \\ \cos\theta & \cos(\theta - \frac{2\pi}{3}) & \cos(\theta + \frac{2\pi}{3}) \\ \sin\theta & \sin(\theta - \frac{2\pi}{3}) & \sin(\theta + \frac{2\pi}{3}) \end{bmatrix} \begin{bmatrix} i_a \\ i_b \\ i_c \end{bmatrix} \tag{2.13}$$

Equation (2.13) shows the general transform matrix for Parks transform for currents. The same matrix may be used to obtain rotor values for flux linkages and voltages. Equation (2.13) can be expressed as a vector:

$$\mathbf{i_{0dq}} = \mathbf{P}\mathbf{i_{abc}} \tag{2.14}$$

where **P** is the transform-matrix derived by Park and Blondel. **P** is a non-singular matrix, because it describes constant rotating flux with constant currents in the fictitious coils. E.g, $\mathbf{P^{-1}} = \mathbf{P^T}$. Calculations can be done with relative ease while in the 0dq-domain. Once the result in 0dq have been reached, the inverse Parks transform, Equation (2.15), can be used to return to stator quantities.

$$\sqrt{\frac{2}{3}} \begin{bmatrix} \frac{1}{\sqrt{2}} & \cos\theta & \sin\theta \\ \frac{1}{\sqrt{2}} & \cos(\theta - \frac{2\pi}{3}) & \sin(\theta - \frac{2\pi}{3}) \\ \frac{1}{\sqrt{2}} & \cos(\theta + \frac{2\pi}{3}) & \sin(\theta + \frac{2\pi}{3}) \end{bmatrix} \tag{2.15}$$

When completing the transform it is noticed that the direct axis and quadrature axis is decoupled, e.g λ_0 is only dependent on i_0, λ_F on i_F and λ_D on i_D. This can be understood by evaluating the way the physical and fictitious coils are oriented

[15, pp. 232]. Attention may now be turned towards the circuit model found by applying the Parks transform on the generator equations. Stator parameters have been converted to direct axis and quadrature axis:

Zero Sequence

$$v_0 = -r\,i_0 - \frac{d\lambda_0}{dt} \tag{2.16}$$

Direct Axis

$$v_d = -r\,i_d - \dot{\theta}\,\lambda_q - \frac{d\lambda_d}{dt} \tag{2.17}$$

$$v_F = r_F\,i_F + \frac{d\lambda_F}{dt} \tag{2.18}$$

$$v_D = r_D\,i_D + \frac{d\lambda_D}{dt} = 0 \tag{2.19}$$

Quadrature Axis

$$v_q = -r\,i_q + \dot{\theta}\,\lambda_d - \frac{d\lambda_q}{dt} \tag{2.20}$$

$$v_Q = r_Q\,i_Q + \frac{d\lambda_Q}{dt} = 0 \tag{2.21}$$

From [10, pp. 438] the variables from Eq. (2.12) becomes transformed to:

$$\lambda_0 = L_0 i_0 \tag{2.22}$$

$$\begin{bmatrix} \lambda_d \\ \lambda_F \\ \lambda_D \end{bmatrix} = \begin{bmatrix} L_d & kM_f & kM_D \\ kM_f & L_F & L_{FD} \\ kM_D & L_{FD} & L_D \end{bmatrix} \begin{bmatrix} i_d \\ i_F \\ i_D \end{bmatrix} \tag{2.23}$$

$$\begin{bmatrix} \lambda_q \\ \lambda_Q \end{bmatrix} = \begin{bmatrix} L_q & kM_Q \\ kM_Q & L_Q \end{bmatrix} \begin{bmatrix} i_q \\ i_Q \end{bmatrix} \tag{2.24}$$

Where $k \triangleq \sqrt{\frac{3}{2}}$. Equations (2.22), (2.23) and (2.24) show the decoupled equations relating flux linkages to currents. The matrix is separated in direct-axis and quadra-

ture axis components, as they are decoupled from each other.

Instantaneous Power Output When operating the generator in steady state, the 0dq-variables can be used to easily express the instantaneous power output of the generator, without having to transform back to abc-variables [15, pp. 235].

$$\begin{aligned} p_{3\phi} &= i_a v_a + i_b v_b + i_c v_c \\ &= \mathbf{i}_{\mathbf{abc}}^{\mathbf{T}} \mathbf{v}_{\mathbf{abc}} \end{aligned} \tag{2.25}$$

From the fact that the Parks matrix is non-singular, $\mathbf{P^{-1}} = \mathbf{P^{T}}$, the power output can be calculated:

$$\begin{aligned} p_{3\phi}(t) &= (\mathbf{P}^{-1}\mathbf{i}_{\mathbf{0dq}})^T \mathbf{P}^{-1}\mathbf{v}_{\mathbf{0dq}} \\ &= \mathbf{i}_{\mathbf{0dq}}^{\mathbf{T}} \mathbf{P}\mathbf{P}^{-1}\mathbf{v}_{\mathbf{0dq}} \\ &= \mathbf{i}_{\mathbf{0dq}}^{\mathbf{T}} \mathbf{v}_{\mathbf{0dq}} \\ &= i_0 v_0 + i_d v_d + i_q v_q \end{aligned} \tag{2.26}$$

2.4 The Mechanical System of a Synchronous Machine

The mechanical characteristics of the synchronous machine are of central importance in power system stability analysis. Rotational inertia equations describe the balance between electromechanical torque (active load) and the mechanical torque (power input from the prime mover) [2, pp. 128]. The turbine and generator acts as a converter of mechanical to electrical energy, and its behavior during disturbances is important to study [15, pp. 533].

Power system stability has been the major concern for power system operators, seeing as stability is vital for secure system operation. Transient instability is the dominant problem in most systems, and receives most of the industry's focus concerning stability [1, pp. 1387]. In later years, the industry introduced the terms *long-term stability* and *mid-term stability*, which deal with stability problems that are not normally covered in the transient analysis [2, pp. 33]. Different forms of

system instability is recognized; voltage stability, frequency stability and inter-area oscillations. Stability can be understood as a *condition of equilibrium between opposing forces* [2, pp. 22]. IEEE/CIGRE Joint Task Force have proposed a definition for power system stability [1, pp. 1388]:

> *Power system stability is the ability of an electric power system, for a given initial operating condition, to regain a state of operating equilibrium after being subjected to a physical disturbance, with most system variables bounded so that practically the entire system remains intact.*

Figure 2.3 is an overview over different classes of power system stability.

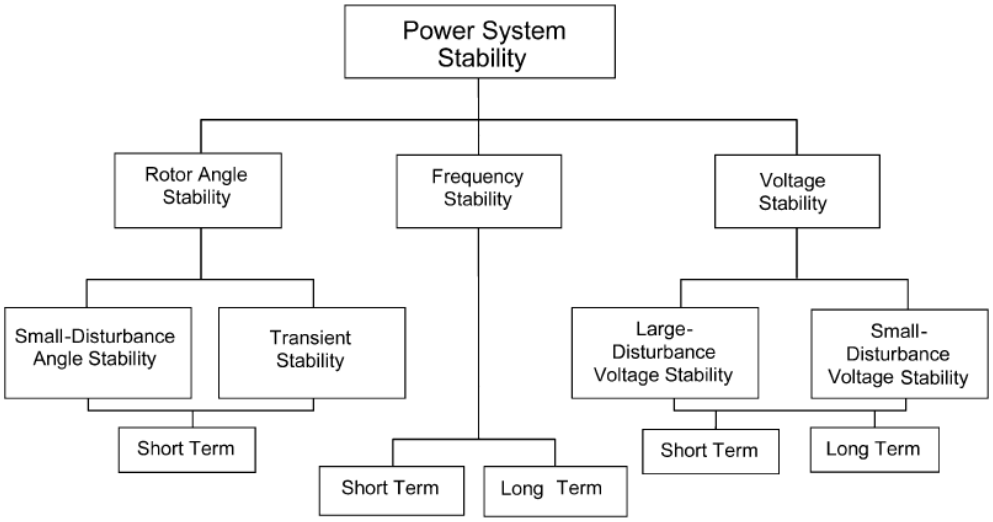

Figure 2.3: Classification of power system stability [1]

Rotor angle stability is used to describe the interconnected system's ability to keep its generators in synchronism during operation, and be able to regain synchronism following a disturbance [2, pp. 18]. The equilibrium between electromagnetic torque and mechanical torque need to be restored for the system to be stable. The mechanical torque is the input torque to the generator, supplied by the prime mover. The electromagnetic torque arises from the load, i.e the currents flowing through the stator windings. The electromagnetic torque opposes the rotation of the rotor. In steady state operation the rotor field and the revolving field of the stator have the same speed [2, pp. 19]. If the system is to be stable, both torque components needs to be present. Lack of synchronizing torque results in aperiodic

drift of rotor angle, while lack of damping torque results in oscillatory instability [2, pp. 23].

Equation (2.27) is called the *swing equation*, and is fundamental in describing rotor dynamics [10, pp. 171]. The swing equation is a non-linear differential equation, that describes the swings in the power angle δ during transients [15, pp. 534]. The equation is based on Newton's second law; it absorbs the moment of inertia of the various parts of the rotor, damping torque and electromagnetic torque. The rotational inertia equations are very important in power system stability analysis as they describe the balance between the torques in every machine [2, pp. 128].

$$M_m \frac{d^2\delta_m}{dt^2} = P_m - P_e - D_m \frac{d\delta_m}{dt} \tag{2.27}$$

where $M_m = J\omega_{sm}$ is the angular momentum of the rotor at synchronous speed, δ_m is the rotor angle in mechanical radians, P_m is the net shaft power, P_e is the electrical air-gap power, and $D_m = \omega_{sm} D_d$ is the damping coefficient. The equation can also be expressed in terms of torques and the *inertia constant H*, as stated by Kundur [2, pp. 131].

$$\frac{2H}{\omega_0} \frac{d^2\delta}{dt^2} = T_m - T_e - K_D \Delta\omega_r \tag{2.28}$$

$$H = \frac{1}{2} \frac{J\omega_{0m}^2}{VA_{base}} \tag{2.29}$$

The inertia constant H is is defined as the kinetic energy in watt-seconds at rated speed divided by the VA base [2, pp. 129]. The inertia constant quantifies the kinetic energy of the rotor in synchronous speed. H is given in seconds, and this is the time it takes for the generator to provide an equivalent amount of electrical energy when operating at rated power output [10, pp. 171].

The main source of damping power in a synchronous machine is the damper windings. These act in a similar way as the squirrel-cage in the induction machine. The dampers act as a screen during subtransient operation, and changes in armature flux can not penetrate them. In transient operation, the air-gap flux which is rotating at synchronous speed induces an emf and current in the dampers whenever rotor speed deviates from synchronous speed. The induced current produces a

damping torque that tries to restore rotor speed to synchronous. This torque is proportional to the speed deviation, and is called *asynchronous torque* [10, pp. 172].

A Power System Stabilizer (PSS) is often include to improve the stability of a system. The basic function of the PSS is to provide additional damping to the rotor. The stabilizer does this by controlling the excitation, using auxiliary stabilizing signals. The PSS produce a component of electrical torque in phase with the rotor speed deviations, thereby it provides damping to rotor oscillations [2, pp. 766].

2.5 Generator Voltage Control

In order to regulate the voltage induced in a synchronous generator, the field current i_F will be altered, as the terminal voltage V_a (here for phase a) is proportional to the delivered field current. The device which delivers the field current to the field winding is called an *exciter*. Controlled by an Automatic Voltage Regulator (AVR), the excitation system maintains the desired voltage output. The power rating of an exciter is usually in the range of 0.2-0.8% of the generators power rating [10, pp.21].

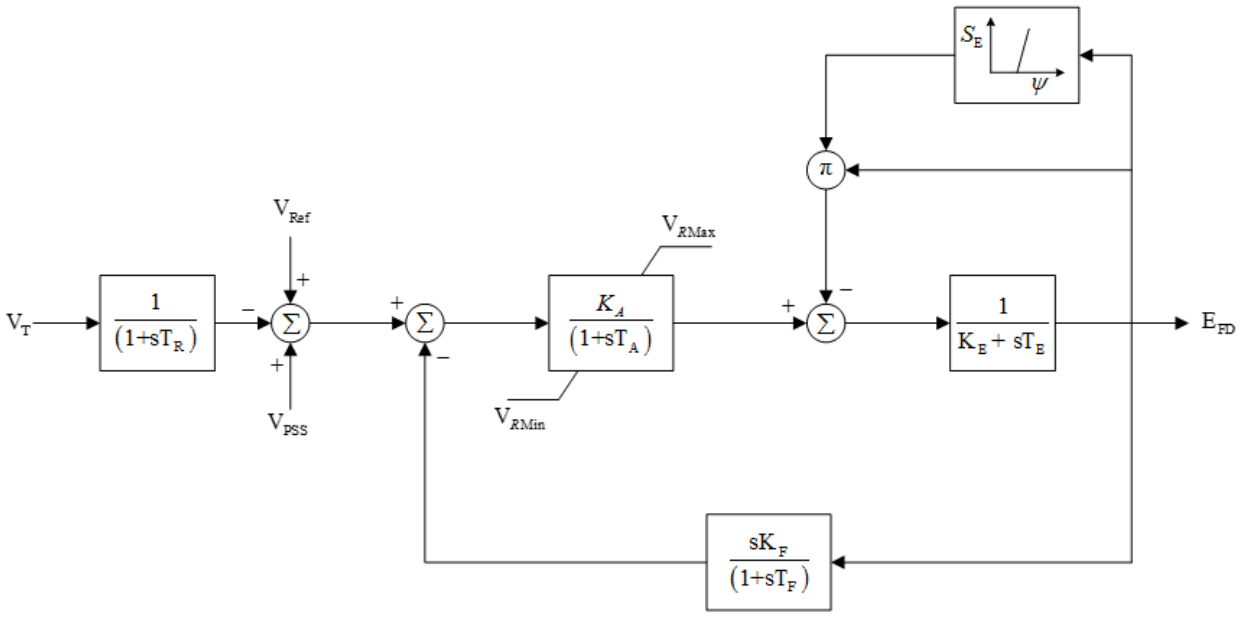

Figure 2.4: IEEE basic blockdiagram of an excitation system

2.5.1 Excitation Systems

Exciter systems can be classified as either rotating or static [10, pp. 22], and this terminology explains how the field is excited. The excitation control system will regulate excitation, as well as provide stabilizing functions. There are three distinctive types of excitation systems available [12, pp. 3]:

- Type DC Direct Current Commutator Excitation Systems
- Type AC Excitation Systems
- Type ST Excitation Systems

Which excitation system would be chosen for a generator depends on cost, size of the machine and local rules and regulations. Common practice is using a rectified AC current feed through slip rings. Figure 2.4 illustrates a basic block diagram of an exciter system. The supply of field current, and an error detector and various feedback loops, complete the AVR [15, pp. 273].

2.6 Load Frequency Control

The flow of active power in a transmission system is closely related to the frequency [2, pp. 581]. The power demand is changing from minute to minute, with peak loads in the morning and afternoon. This affects the frequency, because if there is an imbalance between demand and supply, there will be a drift up or down in the frequency. If power demand exceeds supply, the frequency will fall. Similarly, when supply is greater than demand, the frequency rises. Frequency drift is the main indicator of an imbalance in power generation [24].

In Norway, and most developed countries, the transmission system is interconnected, and is locked to the same electric frequency. This is called a *stiff network*. The entire system work together, and experience a power balance between the units supplying electric power to the grid. Since the first interconnected power systems appeared, the quality of the power system control has been of great concern. It is difficult to define what good control is; can it merely be to keep a constant

frequency? This, of course, is impossible, but system operators strive at keeping an average frequency as close to system reference as possible [25, pp. 650].

In order to meet these fluctuations, there is a need for an spinning reserve generation that can supply power to the bus bars in order to account for a deviation in frequency. For multi-area control to be efficient, it is necessary for all areas in the interconnection to agree on which answers that are important for the AGC. Often, this tends to be a compromise, as there is not a single correct answer to what good control is. Since the bulk of power consumed is during the morning peak, this is often where poor control of power systems is found [25, pp. 650].

When the load increases without altering the mechanical input to the generator, the generator will slow down while trying to compensate for the power mismatch. This is done by an extraction of kinetic energy from the systems inertial storage, which causes the electric frequency to fall because the generator is slowing down [16]. Similarly, when a generator is tripped and the load is disconnected, the lighter loading causes the generator to speed up if the mechanical input is unaltered, and the frequency rises as a result. The load of a power system is ever changing. To preserve the power balance a *unit on regulation* must respond to the changing load by producing more or less power. The objective of the LFC is to maintain a stable frequency while dividing the load between generators, and to control the tie-line interchange schedules [26, pp. 567].

A stable frequency is very important in keeping stability in the network. Many devices depend on a stable frequency in order to operate properly, like the speed output of pumps and fans, and the speed and accuracy of electrical clocks. Induction motors and transformers can be subject to large magnetizing currents should the frequency drop [2, pp.581]. In order to maintain the frequency, utility suppliers make use of Automatic Generation Control (AGC). AGC is a term used to designate the automatic regulation of the mechanical power input to the synchronous generator, to ensure that it operates within a predefined control area [15, pp. 375]. Operators use the AGC both to maintain the frequency and have economically feasible operation. Traditionally, LFC was done manually, and the purpose of AGC is to replace some of the manual control [16]. AGC can reduce the response time to a minute or two, as it reacts to normal load changes. From utility operation there

is no particular reason to speed up the response; neither economic nor control purposes [16].

However, neither manual control nor AGC is able to limit the magnitude of the first frequency deviation following a loss of generation or load in a system [16]. Care needs to be taken with regard to the generating unit characteristics when evaluating an AGC-system, as the performance of the AGC-system is dependent on how the unit responds to such signals. The unit response characteristics may be dependent on various factors, such as [16]:

- Generating unit; fossile-fired, combustion, hydro, nuclear, or combined cycles.
- Fuel; coal, water, oil, gas, or uranium.
- Operation point; Which operation point the unit on regulation is currently on determines the amount of action the AGC can respond with when there is a load change. A unit with the valves wide open can not provide additional response.
- Operator action; unit operators may put the unit under manual control for various operations, such as maintenance.

Hydro units show excellent characteristics to be put under AGC. Low-head hydro units, such as river power plants, show the best response capabilities. They are able cycle over their entire operating range in under a minute. Care must be taken if there are other plants in the same river system, load maneuvering must possible be coordinated with hydro plants up or downstream. High-head units have somewhat slower response time to avoid damage to the penstock due to additional forces from the water in the reservoir [16].

2.6.1 Area Control Strategies

Control areas are separated into: (i) single control area and (ii) multi-area control. In a single area the main input to the AGC is the system frequency. Different strategies can be applied to the AGC; the strategy that yields a generation trend

acceptable in matching the load at the scheduled frequency over the selected time window gets a high score [16, pp. 1108].

The total amount of control is limited in any system, as not all generating units is controllable. Nuclear power plants are almost never put on LFC because they are base loaded to their economical optimal operating point. Gas turbines are rarely put under control. Hydro and fossil generating units are most suited to control, with hydro being most adept. Fossil plants can only be controlled within a small range. Though AGC is an automated and close-looped process, decisions made by human operators affect the performance of the control system. In fact, system operators have to make decisions that all affect the overall performance. Therefore, non-technical causes of error is understood to be human decisions as well as system practice [25, pp. 654].

2.6.1.1 Single Area Control

A strategy that consume less fuel over the selected time window is preferred. Included in this strategy is the ability to avoid undesirable generation ranges, that may include hydro rough spots and problematic steam valve points. The AGC should avoid sustained operation in such ranges.

2.6.1.2 Multi-Area Control

A multi-area consist of several power systems, or "areas", that are interconnected by transmission lines. This operation is a huge benefit, as the different areas are able to support each other if generation in one area is disconnected. The interconnecting tie-lines also opens up for energy exchange, like we see in NPS in Scandinavia. Also, a frequency mismatch measured in one area is an indicator of frequency drift in the entire interconnection. So, if one area tries to correct the frequency drift, it needs a block of generation large enough to correct the power mismatch in the entire interconnection. This again puts constraints on the tie-lines; they have to be able to carry such amounts of power between one area and the others [16, pp. 1108].

If more than one AGC in an interconnection is controlled by a frequency signal,

large power oscillations between control areas will appear if not all areas respond to the error, and regulate simultaneously. There need to be synchronism between all the controllers, the interconnection face severe problems if one controller has a bad measurement error. Then, in the case of a lower value, the area would reduce its generation, causing all other areas to raise theirs. Then both control areas would try to force the frequency to the level they see, causing stability problems [16, pp. 1108].

3 Machine Test Procedures and Parameter Determination

In order to determine performance characteristics of the synchronous machine, it is necessary to conduct several tests. A vast span of articles and publications cover such tests [11, 17, 18, 27–29]. Tests are normally conducted by the manufacturer to provide documentation for the machine before delivery. Field tests are conducted to obtain performance data when the machine has been in service for some time, in order to plan and execute maintenance work. Machine tests cover both salient pole and cylindrical rotor machines, thus with certain assumptions being made to be able to justify the answers [14, pp. 274]. IEEE have produced a guide for test procedures of synchronous machines, which primarily is referred to synchronous *generators* [11]. It can, however, be used to determine parameters of synchronous motors, synchronous condensers and synchronous frequency changers.

Most articles and datasheets mention machine constants. However, there are many different factors affecting the parameters, so a constant will vary with different conditions. The most important factor affecting a machine, is saturation of the magnetic material. Therefore, unless otherwise stated, direct-axis transient reactance, sub-transient reactance and short-circuit time constants are given as saturated values [27, pp. 1333].

3.1 Open Circuit Test

The Open-Circuit Characteristic (OCC) test is used to create the *open-circuit saturation curve*, which is a curve of open-circuit voltage $V_{a,oc}$ as a function of field current I_F when the machine is running in synchronous speed [14, pp. 274]. When the test is performed, record of armature terminal voltage, field current, and shaft speed, or terminal frequency is taken [11, pp. 32].

The open-circuit characteristics represent the relation between the space-fundamental component of the air-gap flux, and the magneto-motive force (mmf) acting on the magnetic circuit when the field winding is responsible for the only mmf source [14,

pp. 274]. Figure 3.1 shows a plot of the open-circuit saturation curve. When the field current is increased, the saturation of the magnetic material increase the reluctance of the flux path in the machine. The result is a reduced effect from the field current when producing magnetic flux, resulting in the sloped terminal voltage curve seen in Figure 3.1 , dubbed occ.

IEEE [11] recommend the following data reading distribution in order to obtain useful data for the generator model:

- Six readings should be taken below 60% of rated voltage, e.g at every 10% of terminal voltage (1 at zero excitation).
- From 60% to 110% tests should be taken at every 5% increment in terminal voltage. This is the critical area where saturation is beginning to have an effect on the open-circuit curve. A minimum of 10 readings must be obtained.
- Above 110%, two readings should be taken as a minimum. Attempt should be made to read at 120% of the rated no-load field current, or at the maximum recommended by the manufacturer.
- At rated voltage, readings should be taken of the line-to-line terminal voltage of all three phases, to check phase balance. These readings should be taken with constant speed and excitation, and with the same voltmeter.

The machine should be allowed to run for several minutes at each voltage point to allow the speed of the generator to stabilize at the rated value. This ensures that there will be no variation in speed and excitation, causing no error in the measurement. In the open-circuit test, readings should be taken with increasing excitation, as this method of measuring allows for an initial energization of the generator. If it is necessary to take another measure of a voltage point, the excitation will have to be turned to 0 % then raised carefully to the desired point. This eliminates the effect of hysteresis [11, pp. 33]. With the armature terminals open-circuited, the terminal voltage is equal to the induced emf E_{af}. The results of this test can then be used to measure the relationship between I_F and E_{af}, and therefore provide a direct measurement of the field-to-armature mutual inductance L_{af}. In Figure 3.1 the first part of the curve is linear. This is called the *air-gap line*, and represent the

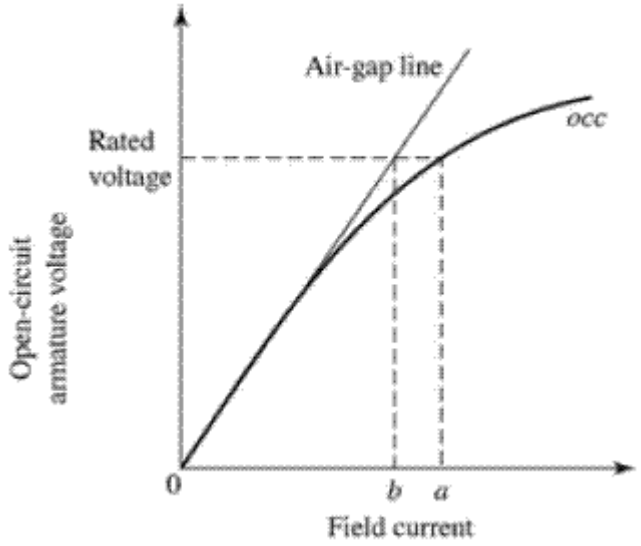

Figure 3.1: Open-circuit characteristics of a synchronous machine [14]. Prefix b reveals the unsaturated field current $I_{f,u}$; a is the saturated field current $I_{f,s}$. $o\,c\,c$ is the open-circuit curve.

machine open-circuit voltage characteristics corresponding to unsaturated operating conditions. This means that the air-gap is the dominant reluctance in the flux path. In operation, the magnetic material become saturated; necessitating a higher excitation current to achieve the same rated voltage [14, pp. 275]. It is common to determine machine parameters when operating with no saturation, and referring all quantities to the air gap line [19, pp. 516].

If a measurement of the mechanical power can be obtained during the test, the machine's *no-load rotational losses* can be determined. When the generator is unexcited, the power required to drive the machine at synchronous speed is its friction and windage loss. To find the core losses, the generator is excited and driven at synchronous speed. The power is then equal to core loss, windage loss and friction loss [14, pp. 276].

3.2 Sustained Short-Circuit Test

The Sustained Short-Circuit (SSC) test is performed to find the *short-circuit characteristics curve* and *load losses* in a synchronous machine. The short-circuit characteristics is a curve of short-circuit terminal current $I_{a,sc}$ as a function of the field

current, and is obtained by applying a solid three-phase short-circuit to the armature terminals of a synchronous machine driven at synchronous speed [14, pp.276].

$$X_{s,u} = \frac{E_{aaf0}}{I_{a0}} \tag{3.1}$$

where $X_{s,u}$ is the unsaturated synchronous reactance, E_{af0} is the unsaturated generated voltage in rms induced by the field current I_{f0}, and I_{a0} is the armature current that is the result of the same field.

$$X_s = \frac{V_{a,rated}}{I'_a} \tag{3.2}$$

where X_s is assumed equal to the saturated synchronous reactance, $V_{a,rated}$ is the open-circuit voltage, and I'_a is the armature current read from the short-circuit characteristic at I_F=Amperes Field No Load (AFNL).

$$X_{s,u} = \frac{I_f}{AFSC}\,[perunit] \tag{3.3}$$

where Amperes Field Short Circuit (AFSC) is the value of the field current which produces rated short-circuit current in 1.0 per unit. Following, I_f=AFNL, E_{af}=$V_{a,rated}$= 1.0 per unit and

$$I'_a = \frac{AFNL}{AFSC}\,[perunit] \tag{3.4}$$

From Equation (3.2) the saturated synchronous reactance can be calculated:

$$X_s = \frac{V_{a,rated}}{I'_a} = \frac{AFSC}{AFNL}\,[perunit] \tag{3.5}$$

The Short-Circuit Ratio (SCR) is defined as the ratio of AFNL and AFSC, and is the inverse of the per-unit saturated synchronous reactance

$$SCR = \frac{AFNL}{AFSC} \tag{3.6}$$

By applying test output values to Figure 3.2, and using Equation (3.2) the syn-

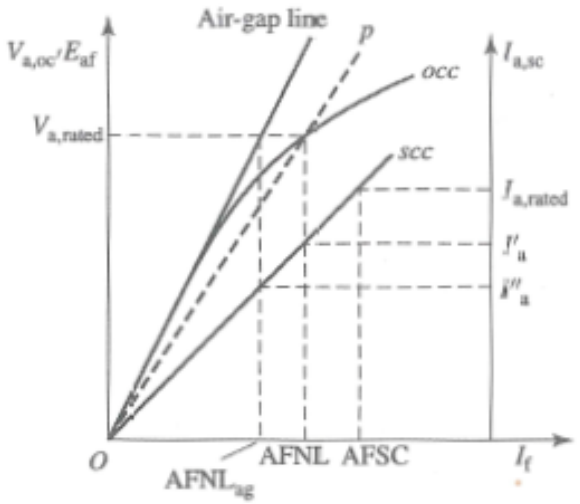

Figure 3.2: Open- and short-circuit characteristics of a synchronous machine [14]. The figure is showing the equivalent magnetization line for saturated operating conditions.

chronous reactance X_s can be calculated.

3.3 Slip Test

The slip test is used to determine X_d and X_q in a practical manner, and it has been covered in several papers and standards [11, 19, 27]. The rotor of the synchronous machine is driven at a speed that is slightly different from the synchronous speed. The field is kept open-circuited, while a balanced, three-phase, rated-frequency, positive-sequence power source is energizing the armature. The voltage is kept below the point on the open-circuit curve where the saturation curve deviates from the air-gap line, i.e. in the linear area. The purpose of the test is to let the poles slip past the mmf wave, thus the magnetizing current will be a function with respect to the mmf [19, pp. 516–517]. Oscillograms is taken of armature voltage, armature current and field voltage [11, pp. 99]. As the pole position changes, the current and voltage will modulate, the variation in voltage is because of reactance drop in the power source used. When the poles line up with the axes of the phases, the current is minimum. By taking the ratio of voltage to current, the direct synchronous reactance can be determined. When the axes of the phases are midways between the poles the same ratio gives the quadrature synchronous reactance [19, pp. 517].

3.4 Armature Leakage Reactance of the Stator

Substantial work has been put in to the research to give an accurate calculation of the stator leakage reactance, which is a crucial parameter for machine designers and operators [30–32]. The traditional way of calculating this reactance was by using the Potier-method. However, early work by L. A. Marsh and S.B. Crary showed that the Potier-method, when performed at rated values of the machine, could yield errors up to 100 % between the Potier-reactance (calculated) and the stator leakage reactance (actual) [32, pp. 381]. The armature leakage reactance of the stator is typically in the range of 10 % of the synchronous reactance [14, pp. 273].

3.4.1 Potier-method

The Potier-method uses the OCC, along with the Zero Power Factor Characteristic (ZPFC) for the synchronous machine [11, 32]. Figure 3.3 show how the OCC and the zero power factor curve is being used to find the Potier-reactance. The ZPFC-curve is found by running the synchronous machine as an overexcited generator with a purely inductive load. This can be done by using reactor banks, or to have a connection to a load of idle-running, unexcited synchronous machines [11, pp. 36]. To create the zpfc-curve, proper tuning of the excitation current for the machine under test allows the operator to have different values of terminal voltage, while maintaining constant armature current for the synchronous generator being tested. The ZPFC is a plot of terminal voltage against field current [11, pp. 36]. The Potier-reactance is found as such [11, pp. 54]:

- Rated voltage is given as 1 p.u. The intersection between rated voltage and the zero power factor curve gives point *d*.
- The length *ad* is the length of the field current necessary to produce rated current in the SSC-test. This field current is similar to the current needed to produce zero voltage on the zero power factor curve.
- From the point *a*, a line parallel to the air-gap line in the OCC-curve is drawn. The intersection of this parallel line with the saturated open-circuit curve

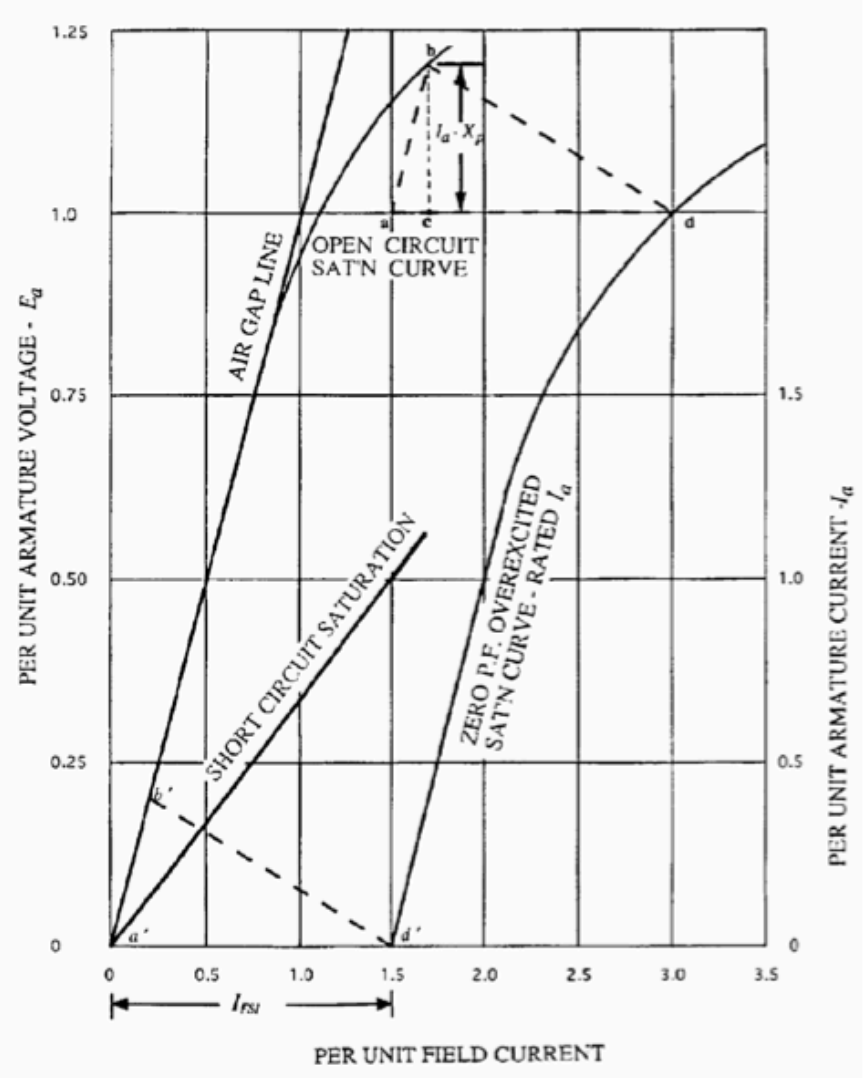

Figure 3.3: Determination of the Potier-reactance [11], using typical curves found in synchronous machines.

gives the final point *b*.

- The vertical distance from point *b* to the line *ad* expressed in per unit, is equal to the rated p.u. armature current times the p.u. Potier-reactance. The mathematical expression is given in Equation (3.7).

$$E_b - E_d = I_a \times X_P \tag{3.7}$$

Where E_b is the voltage at the intersection of the open-circuit curve, and the parallel air-gap line. E_d is rated voltage, at 1 p.u. I_a is rated current, and X_P is the Potier-

reactance.

The problem with the Potier-reactance is the relative high rate of inaccuracy. Figure 3.3 clearly show that the placement of the Potier triangle will affect the size of the reactance. For rated voltage, the triangle will be located in the knee of the open-circuit characteristic that gives the tangent of the OCC a high value. By increasing the excitation on the zero power factor test, the armature current is also raised due to the machine moving into saturation. The Potier-triangle will then have a much lower slope. Case-studies show that the Potier-reactance approach the leakage reactance at high values of saturation [32, pp. 380]. That is, for salient-pole machines only. In cylindrical rotor machines the Potier-reactance is almost constant, due to a small amount of field leakage flux and flux distortion. March and Crary propose that as high a value of field current as possible should be applied during the test to correctly determine the leakage reactance [32, pp. 381]. To achieve accurate results it may be necessary to apply 1.4 times the rated voltage. Conducting measurements at these levels of voltage could be hazardous for the machine under test [31, pp. 284].

3.5 Signal Conditioning

The output most measurement devices, called conditioning elements, are either a dc voltage, dc current or a variable frequency ac voltage [33, pp. 247]. Calculations are performed on these variables to establish the value of the signal that is measured. To a large degree, electric power measurements are haunted by harmonic noise. Filters are essential in obtaining the measured signal. Shielding of wiring and devices also prevent noise from corrupting measurement data.

3.5.1 Signal Filtering

Measurements in power stations, and around synchronous machines tend to be very noisy, due to high harmonics and electromagnetic interference [34, pp. 408]. In order to obtain the raw signal, and discard the interference, filtering is necessary. A filter can be either analog or digital, and transmits a certain range of frequency,

while rejecting all others [33, pp. 117]. In [34, 35] a median filter was applied to a sudden short-circuit test. This filter made it possible to enhance the measured signal, without smoothing out the edges.

3.5.2 Uncertainty in Measurements

The electric machines generate heat when they operate, this alters the parameters of the machines. This is called a *bias error*.

The uncertainty in the measurements is connected to the measured result, even though this uncertainty may be caused by the devices or instruments used in the test. Calibration of instruments, and heat generation are two factors that cause uncertainty in the output quantity. The Guide to the expression of uncertainty in measurements (GUM) method is a renown method for calculating uncertainty in measurements [36, pp. 135].

The estimation of uncertainty is dependent on how precise the measurements is required to be. If the requirements for accuracy is very high, the input and output variables must be described accurate, so all essential contributions is accounted for. Equation (3.9) is used to describe the standard uncertainty [36, pp. 148–149].

$$\bar{x} = \frac{1}{n}\sum_{j=1}^{n} x_j \tag{3.8}$$

$$u(\bar{x}) = s(\bar{x}) = \sqrt{\frac{\sum_{k=1}^{n}(x_k - \bar{x})^2}{n(n-1)}} \tag{3.9}$$

Where X the input quantity, and x_j is the observed median for this variable. n is the number of independent observations. $s(\bar{x})$ is the standard deviation. Equations (3.8) and (3.9 are used when the measurements are independent.

4 Generator Control System

The definition of a control system according to N. Nise is: a combination of subsystems assembled for the purpose of obtaining a desired output with a desired performance when given an input [21, pp. 2]. The history of control systems goes back to the Greeks in 300 B.C, when they controlled liquid flow to measure time using a feedback system [21, pp.4]. Control system engineering as we know it today was developed in the late 1800s and mid-1900s. Prominent names include E.J Routh, J.C Maxwell, A.M Lyapunov, N. Minorsky, H.W Bode, H. Nyquist and W.R Evans.

Control systems are separated into two categories: (i) open-loop system and (ii) closed-loop system. In AGC for example, a closed-loop system is used to alter the mechanical input to the generator. These systems have the ability to correct any deviation from the desired output, by using a *feedback loop*. Advantages in using a closed system is greater accuracy and less sensitivity to noise, disturbance and changes in the environment. A feedback loop enables the system to "learn" from previous changes. The output signal is taken back via the feedback loop, subtracted from the input, the resulting signal is called *actuating signal*. If the output is correct, then the feedback does not affect the signal, the system only makes changes to the gain when the signal deviates for the *set value*. A control system responds to an input by undergoing a transient response before the output settles at a steady-state that resembles the input; this is called *dynamic behavior* [21, pp. 10].

4.1 Transient Response, Steady-State and Stability

Transient response is a term used to describe how *fast* the system alters. This is important, and different for every control system. A fast transient response can cause damage to structures, say a violent opening of a valve causes a shock to the turbine and generator, which can result in bending and fracture of the turbine blade. A slow response, although safe, will in some cases result in a very slow system. The response might be too slow, and the system will never reach its proper balance.

The steady state response is how accurate the system can resemble the desired

input. *Steady-state error* is a term used to describe the deviation from desired value. Example may be an elevator that is at the third floor, the doors needs to open at an elevation that enables safe exit for the passenger. In order to evaluate the stability of a system, it is necessary to look at the total response; e.g the sum of the *natural response* and *forced response*. The natural response depends on the system alone, it tells how the system dissipates or acquires energy [21, pp. 11]. The response of most systems is described by differential equations. The Laplace transform is introduced to simplify calculations of these solutions. Equation (6.20) show a typical Transfer Function (TF) solved in the Laplace plane. This TF is a first order function. For higher order there will be a Laplace operator, s, in both the denominator and the numerator.

$$G_g(s) = \frac{1}{1 + s\,T'_{do}} \tag{4.1}$$

To evaluate the output of a TF, the differential equation or Laplace equation can be solved. However, a more rapid and qualitative method presents itself. By inspecting the function, results can be derived in a minimum of time. This technique bases itself on poles and zeros, and their relationship to the time response of the system. The *poles* of a TF are the value of the Laplace transform variable, s, that projects the TF towards infinity. It can also be the roots of the denominator that are common to the roots of the numerator. The *zeros* of a TF is the value of s that causes the TF to become zero. It is also the roots of the numerator that are common to the roots of the denominator [21, pp. 162–163].

4.1.1 Stability of a Control System

Stability is one of the most important system features. The question that arises is: will the system be able to regain its steady-state operation, following a disturbance? A system is stable if the natural response approaches zero as time goes to infinity; unstable if the natural response increases without limitations as time goes to infintity; and marginally stable is the natural response neither grows nor decays as time goes to infinity [21, pp. 302].

The Routh-Hurwitz Criterion is a quick and simple technique that yields informa-

tion about the stability of a system, without having to solve for the closed-loop poles. It is a two-step method: (i) first the Routh Table is generated; (ii) then the table is interpreted. The table yields information of how many poles that are in the left half-plane, right half-plane or on the $j\omega$-axis. The TF needs to be closed, then it is a matter of evaluating the terms in the denominator. Herein lies the strength of the Routh-Hurwitz criterion, it can be used to design a range for the parameters that will ensure stability [21, pp. 305].

Root Locus is another method of analysis that can be used on closed-loop systems. It yields a graphical presentation of the closed-loop poles, and can therefore be used to examine stability. The real power of the Root Locus is the ability to solve systems of higher order than 2. The best way to obtain the Root Locus of a closed-loop system is by using software like Matlab. If it is desirable to draw by hand, this can be achieved by following instructions in [21], pp. 397-410. Graphically, the locus is drawn in the complex plane. For most systems, the poles are located in the left half-plan up to a particular value of gain. If gain is increased, the poles will move into the right half-plan. The system then becomes unstable. The root locus can also be used to design % overshoot, settling time and peak time, to mention some [21, pp. 388–405].

4.2 Second-Order Systems

Most control systems are of a higher order. However, most systems can be modeled as a second-order system. The technique of *Zero-Pole Cancellation* allows third-order systems or higher to be approximated as a second-order system [21, pp. 194], with acceptable accuracy. A second-order system have two particular quantities which are meaningful when the system is specified. This is the natural frequency and damping ratio [21, pp. 173]. The natural frequency is the frequency of the oscillation when the system is not damped. The damping ratio is a measure of the nature of the transient; how much overshoot and damping of oscillations the transient contains.

Four different second-order systems are encountered [21, pp.172]:

- Overdamped Response: Two real poles at different location in the left half plane. The natural response is two exponentials with time constant equal to the reciprocal of the pole location.
- Underdamped Response: Two complex poles. The natural response is a damped sinusoid.
- Undamped Response: Two imaginary poles. Experiences undamped sinusoid.
- Critically Damped Response: Two real poles at almost same location in left half plane. The natural response is a combination of an exponential with a time constant equal to the reciprocal of the pole location. The other term is the product of time and the exponential time constant of the other pole.

The different responses are illustrated in Figure 4.1.

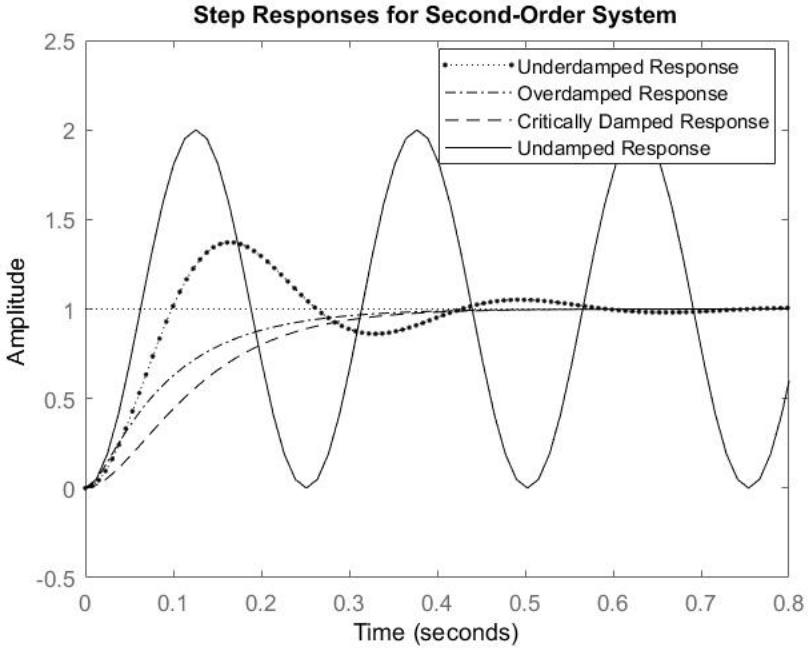

Figure 4.1: Step response for second-order systems with different damping [21, pp. 173]. The first transfer function is the underdamped response, the second is the overdamped response, followed by the critically damped response and the oscillating undamped response.

4.3 PID Controller

The classic controller used in control systems is the PID-controller. It is a three-step controller that envelops changes over past and future time to reach an optimal set-point. Much of the theory behind the PID-regulator is attributed to Nicholas Minorsky.

A PID controller evaluates past error, present error and future error when making adjustments to the system. [37, pp. 436]. The generic TF for a PID controller is given in Equation (4.2).

$$G_{PID}(s) = k_R \times \frac{T_i s + 1}{T_i s} \times \frac{T_d s + 1}{1 + \frac{T_d s}{n}} \tag{4.2}$$

Where k_R is the controller gain, T_i is the integration time, T_d is the derivative time, and n is a factor used to remove the derivative effect at high frequencies. Compliance with given tuning rules approximates this with $n = 10$.

The PID-regulator can be described as follows [38]:

4.3.1 Proportional

The Proportional controller is affecting the actuation by multiplying the error from set value by a gain k_p. The controller tries to reduce the error in real-time. The gain is reduced when the system is approaching reference value, but this point will never be reached with only a P-controller.

$$u = k_p \times e = k_p \times (r - y) \tag{4.3}$$

The measure of proportional response is called *sensitivity*, and adjustment of this is necessary to attain optimum stability [20, pp. 759]. The P-controller commands the actuator to respond to the error. A high gain will make the system unstable, and it will start oscillating [37, pp. 436].

4.3.2 Integral

The Integral controller notices all previous errors in the system. The controller integrates the error, and use the result to affect the actuation with the gain k_i. The I-controller eliminates the stationary error in a system.

$$u = k_p \times e + k_i \int e(t) d\,t \tag{4.4}$$

To much gain on the I-controller will also cause oscillations.

4.3.3 Derivative

The Derivative controller changes the actuation by taking the time-derivative of the error, and multiply this with the gain k_d. Now the controller is able to predict how much gain is needed to reach the set value based on the shape of the actuating function.

$$u = k_p \times e + k_i \int e(t) d\,t + k_d \times \frac{d\,e(t)}{d\,t} \tag{4.5}$$

The derivative gain increases the stability of the system, but it slows down the response [37, pp. 436].

All the previously mentioned parameters have to be tuned if the system is to be stable after regulation. A number of techniques exist to do this, such as the Ziegler-Nichols method, Cohen-Coon tuning method, Internal Model Method, Tyreus-Luyben Method, to mention a few [37, pp. 436]. These tuning rules were created to save time for engineers, when setting the controller in a practical setting. Thus, it was possible to quickly arrive at the optimum setting for the controller [20, pp. 759].

5 Method

The objective of the thesis is to verify and test the synchronous generator machine rig acquired by Western Norway University of Applied Science in a quantitative way. The various parts of the machine rig will be subjected to a step in speed and/or subjected to a change in load. The step response will then be used to design transfer functions. Next, an attempt will be made to design a controller to regulate running speed of the generator.

The various tests will be performed on a Terco MV1027-235 salient pole synchronous machine. The principal tests are: (i) OCC; (ii) SSC; and (iii) the slip test. These tests will verify the electric parameters of the generator. Part two of the thesis will be dedicated to the design, testing and stability of the control system. This will be done experimentally, and results will be recorded and processed. Special focus will be given to the mechanical system, and the control of active power generation.

The machine rig consist of a prime mover machine, a Terco MV1054 Digital Torque, Speed and Shaft Power meter, and the synchronous machine.

Table 2: Synchronous machine nameplate

Synchronous Machine 3-phase MV1027-235	
Generator: 1.2 kVA 0.8	Ser. No: 39333
Motor: 1.0 kW	Temp. C: F (155°C)
Y 220-240 V 3.5 A	Protection (IP23)
Δ 127-140 V 6.1 A	Duty Type S2 60 min
Excitation DC 220 V 1.4 A	Norm: EN 60034:1993
50 Hz 1500 rpm	ISO 9001

5.1 Prime Mover

The prime mover is represented by a electric machine connected to the synchronous machine. An analog 0-10 VDC signal will be used to control the speed of the prime mover. The step in mechanical power output from the prime mover will be given as a step in voltage.

The voltage step is planned delivered by a two channel 0-30 VDC power supply. The channels will be separated by a power diode, which feeds the channel with highest voltage to the drive. The channel with the lower voltage rating is connected to the anode of the power diode. The higher rated voltage source is connected to the cathode, separated by a switch. When the switch is turned, the high rated voltage source begins to supply the analog input of the drive. The power diode blocks the lower voltage source. The setup is shown in Figure 5.1.

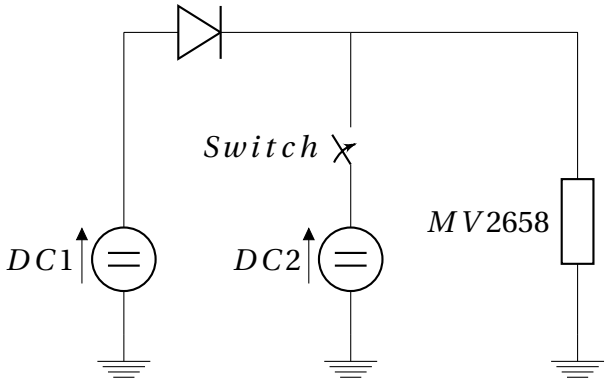

Figure 5.1: The circuit that delivers the step to the Terco MV2658 PWM Control Module. DC1 is the source with lower voltage. When the switch is turned, DC2 start to supply the drive. The diode will then start blocking the voltage from DC1, since this voltage is lower than DC2.

5.1.1 DC Machine

The dc machine is a versatile machine, and is capable of operation over a large range of speeds. The dc machine will be employed as the prime mover in the OCC and SSC tests, and in experimental step response experiments. The Terco MV1028-225 dc machine used is controlled by the Terco MV2658 PWM dc control module. The machine rating is given in Table 3. The PWM dc Control Module supplies a constant field voltage and constant field current, and a variable armature voltage. Regulation of armature voltage can be done either with a potentiometer located on the MV2658, or with an 0-10 V analog signal fed into the external control input. Thus, the first experiments was performed with the two dc-sources to effect the step. The step was delivered to the MV2658, which then was used to control the dc machine (see Figure 5.1).

Table 3: DC machine nameplate

DC Machine MV1028-225	
Generator: 2.2 kW 1500 rpm	Ser. no: 39329
Motor: 2.0 kW 1500 rpm	Temp. C: F (155°)
Rotor: DC 220 V 12 A	Protection: (IP23)
Excitation: DC 220 V 0.8 A	Duty Type: S2 60 min
	Norm: EN60034:1993
	ISO 9001

The dc machine has a duty type S2 60 min rating, which is a short time duty cycle [39, pp. 2]. IEC has defined this in NEK IEC 60034-1:2010. This means that the machine can run for 60 minutes, before the machine must rest until it regains ambient temperature.

5.1.2 Induction Machine

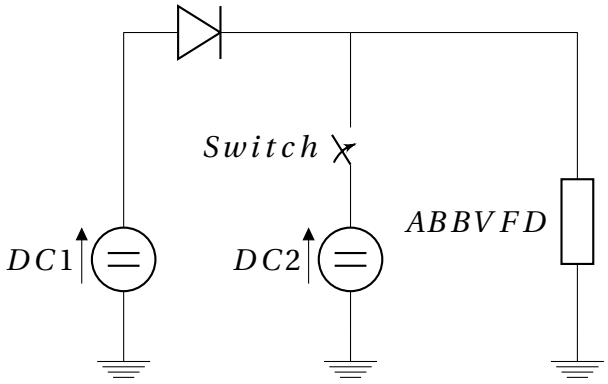

Figure 5.2: The circuit that delivers the step to the Variable Frequency Drive (VFD). DC1 is the source with lower voltage. When the switch is turned, DC2 start to supply the VFD. The diode will then start blocking the voltage from DC1, since this voltage is lower than DC2.

For the slip test the results depend on a constant speed. A Terco MV009 induction machine was used as a prime mover, as a supplement to the dc machine. This machine is going to be employed in experiments to determine the dynamic response of the system. The induction motor will then be controlled by a PID controller. The induction machine is suited to continuous testing, as it is provided with a fan and heatsinks, which eliminates the problem of heat dispersion.

An ABB ACS880-01 VFD controls the induction machine. An analog 0-10 VDC signal

Table 4: Induction machine nameplate

Induction Motor M3AA 090LB-4 IE2					
3GAA092520-ASE IEC 60034:1					
V	Hz	rpm	kW	A	cos ϕ
230 D	50	1435	1.1	4.1	0.78
400 Y	50	1435	1.1	2.4	0.78
460 Y	60	1740	1.1	2.1	0.76
Temp C: F	IP55				

to the drive will be used to control the speed of the induction machine. The ABB Drive Composer is a computer program that is used to alter the default settings of the drive, and to determine the span of revolutions per minute that will be altered by the 0-10 VDC signal.

5.2 Open-circuit and Short-Circuit Characteristics

For the OCC- and SSC-tests, the synchronous machine is to be left running at synchronous speed. The prime mover is a PMW-controlled DC machine. For each measurement point taken during the tests, the speed will be adjusted to synchronous speed 1500 rpm.

The open circuit curve will be created by taking six recordings from below 60 % of rated voltage, with one at zero excitation. The generator is left open-circuited, the field being energized by a Langlois Kompak40 dc source. The terminal voltage shall be collected by a Fluke 235 Power Quality Analyzer. Field voltage and field current is measured with two Hioki multimeters. From 60 % to 110 % measurements will have a 5 % increase in terminal voltage, record is scheduled for 13 points above 60 % rated voltage, as recommended by IEEE [11].

The excitation current is increased slowly from 0 % excitation, and the machine must be left running at each measurement point to let the speed stabilize. This is the recommended way to perform the open-circuit test [11, pp. 33].

The short-circuit curve is obtained by running the machine at synchronous speed, with a three-phase solid short-circuit at the armature. The short-circuit will be

created by connecting wires from a neutral point to each of the three armature connections, while keeping a wye-connection. Three Fluke i5s current clamps will measure the short-circuit current, the result shall be read off the Fluke 235 Power Quality Analyzer.

The SSC curve is plotted using recordings of field current and short-circuit current that is found in the test. A total of six recordings will be taken, at 0 %, 25 %, 50 %, 75 %, 100 % and 125 % of rated current. The readings are best captured with decreasing excitation, so that the highest short-circuit current is taken first. This ensures that the winding temperature is nearly constant during the test, which is recommended [11, pp. 34–35].

Two methods of determining the synchronous reactance for the Terco machine can be used; one in which calculation is based on the field current when reaching rated voltage in the open-circuit test, and rated current in the short-circuit test. The other method based the calculation on the value of armature voltage and armature current when a field current of any value was applied to the synchronous machine running at rated speed [27, pp. 1335].

5.3 Potier Reactance test

The first step of finding the Potier reactance is to use the OCC-curve previously found in the open-circuit test. The next step is to find the ZPFC. Line-to-line values of voltages are obtained, so a mean value of all three phases will be calculated to determining the OCC and Potier-reactance.

5.3.1 Zero Power Factor Characteristics

This curve is found by loading the generator with an inductive load. For this test various inductive loads can be used, and the load that draws the least active power should be used to complete the calculation. The various loads available is an Elektrotechnische Werkstätten Hof (EWH) synchronous machine, Terco MV1101 Reactance Load and an ASEA reactive load.

Starting off, the synchronous generator is running at rated speed, delivering rated current to the load. An attempt will be made at delivering rated current to the load, with terminal voltage equal to zero. Then the field current at zero volts at the terminals would have been equal to the field current needed to deliver rated current in the SSC.

The first data will be collected with a very large reactance. The excitation must be increased until rated current is achieved. Measurements are collected with a Fluke Power Quality Analyzer and two Hioki multimeters. Thereafter the reactance will be reduced and the excitation raised, while keeping the armature current at rated level. An reactor unit from Asea is utilized. It has a potentiometer-style regulation, measurement points will therefore be random selected. The terminal voltage on the synchronous generator will increase as excitation is raised. For the sake of the test, it is the points with high terminal voltage that is of interest when locating the Potier reactance. The ZPFC is a plot of terminal voltage and field current from this test.

The test is completed when rated values for field voltage and field current on the synchronous machine is reached. The experiment is ended before harmful voltage and current is delivered to the field winding.

5.3.2 Potier Triangle

The OCC and ZPFC curves will be sketched in the same plot in Matlab. The mean of the phase voltages is selected in accordance with test procedures [11]. It must then be converted to line voltage. A straight line is plotted in the same figure at rated line-to-line voltage 230 V. This line crossed both the OCC and the ZPFC. These intersection points are dubbed *a* and *d*.

From point *a*, a line which is parallel to the *air-gap line* is drawn. This is a straight line, and it crosses the OCC when the effects of saturation bends the curve. The intersection between these two lines is called point *b*. Points *a*, *b* and *d* form the Potier-triangle.

5.4 Slip Test

The synchronous machine under test is regulated so that it is running slightly slower than rated speed, from 1 % to 4 % below synchronous speed. The field winding is left open-circuited. A positive, three-phase 50Hz power supply (Langroise) will be connected to the armature of the machine at test. Constant speed is a precursor for being able to perform the slip test. The experiment setup consisted of the synchronous machine under test connected to a induction machine via the torquemeter. The Terco MV1009 induction machine is controlled with an ABB ACS880-01 drive, ensuring constant speed during the experiment.

Measurement data is collected with the Picometer 4824 digital oscilloscope. Three Fluke DP120 differential voltage probes collected the line voltages, being set at a resolution of 200x. A fourth Fluke DP120 is used to collect the field voltage, a Hioki multimeter was also connected to the field winding to enable the author to monitor if harmful voltages arose in the field. The armature currents were measured with three Fluke i5s AC current clamps, which have a resolution of 400 mV/A.

Two tests will be performed, the first with a slip of 1 %, the generator running at 1485 rpm. 25% of rated line voltage, 57 V, is applied to the armature, as recommended by Wright [27, pp. 1334]. Another test will then be performed, with the machine subjected to a 4 % slip, running at 1440 rpm. Again, 57 V will be supplied to the armature. Readings will be taken with the Picometer 4824, having a sample rate of 1 MS. Sample time desired is five seconds.

5.5 Prime Mover Experimental Step Response

The experimental step response will be obtained by evaluating the response of the two systems: (i) the mechanical prime mover and (ii) the electrical synchronous generator with load. Nominal values are chosen for the synchronous generator, as stated on the nameplate. Data recording with the Picometer 4824 digital oscilloscope will include: (i) speed measurement; (ii) torque measurement; (iii) armature current; (iv) input step signal; (v) excitation current; (vi) excitation voltage; and (vii) time. A Fluke 435 Power Quality Analyzer will also be connected to the armature of

the synchronous machine, to examine the power drawn by the load. Three Hioki digital multimeters is available to observe various voltage levels. The step voltage will be applied with the setup described in Figure 5.1.

The mechanical prime mover response is found by removing the synchronous generator from the machine rig. The prime mover is powered from the ABB 880 VFD with respect to the asynchronous machine, and the Terco PWM with respect to the dc machine.

The VFD is controlled in two ways: (i) speed control; or (ii) frequency control. When placed under speed control, an internal PID would maintain the speed chosen by the operator. In frequency control, the operator would select the frequency delivered to the induction motor, i.e the speed. This setting did not have a controller regulating speed, with respect to loading and such. A feedback loop was included in the tests with the loaded synchronous generator, between the VFD and the Terco MV1054 Digital Torque, Speed and Shaft Power meter.

5.5.1 PID Controller Tuning

Various techniques for tuning the PID controller exist, where each method serves a design objective. This thesis employ a reaction curve based method, as proposed by Ziegler and Nichols, and their peers as its first and foremost method [40, pp. 166]. A frequency response tuning method is also applied. The goal is to set the PID controller so a 4:1 damping is obtained in the system, i.e that the first and second peaks have a 4:1 ratio in overshoot. Before tuning can commence, a model of the process in open loop is required. Sampling of data will run over 20 seconds. Once a step is given, the dynamic response will allow to run until a new steady-state is reached. The general transfer function for a PID controller is given in Equation (5.1). This transfer function is then included in the open loop for the system under investigation before the system process. Then the loop is closed, and stability criteria can be investigated.

$$G_{pid}(s) = k_R \times \frac{(T_i s + 1)(T_d s + 1)}{T_i s(1 + \frac{T_d s}{n})} \tag{5.1}$$

Where k_R is the controller gain, T_i is the integration time, T_d is the derivative time, and n is a factor used to remove the derivative effect at high frequencies. Compliance with Ziegler-Nichols is achieved when setting $n = 10$.

5.5.1.1 Reaction Curve Tuning Rules

The process reaction curve will be captured with an oscilloscope. The system is left in open loop when a step is given. The response is captured until it reaches its steady state. The reaction curve is then created by drawing the maximum slope tangent of the curve [40, pp. 166]. Equations (5.2), (5.3) and (5.4) is calculated by evaluating the reaction curve of the system. These parameters will be used in the tuning rules described later in this section, to determine possible controller settings.

Table 5 show the settings that comply with Ziegler-Nichols, while Table 6 show Cohen-Coon's proposed settings.

$$K_0 = \frac{y_\infty - y_0}{u_\infty - u_0} \tag{5.2}$$

$$\tau_0 = t_1 - t_0 \tag{5.3}$$

$$\nu_0 = t_2 - t_1 \tag{5.4}$$

Table 5: Ziegler-Nichols tuning with reaction curve

	K_P	T_i	T_d
P	$\frac{\nu_0}{K_0\tau_0}$		
PI	$\frac{0.9\nu_0}{K_0\tau_0}$	$3\tau_0$	
PID	$\frac{1.2\nu_0}{K_0\tau_0}$	$2\tau_0$	$0.5\tau_0$

Table 6: Cohen-Coon tuning with the reaction curve

	K_p	T_i	T_d
P	$\frac{\nu_0}{K_0\tau_0}\left[1+\frac{\tau_0}{3\nu_0}\right]$		
PI	$\frac{\nu_0}{K_0\tau_0}\left[0.9+\frac{\tau_0}{12\nu_0}\right]$	$\frac{\tau_0[30\nu_0+3\tau_0]}{9\nu_0+20\tau_0}$	
PID	$\frac{\nu_0}{K_0\tau_0}\left[\frac{4}{3}+\frac{\tau_0}{4\nu_0}\right]$	$\frac{\tau_0[32\nu_0+6\tau_0]}{13\nu_0+8\tau_0}$	$\frac{4\tau_0\nu_0}{11\nu_0+2\tau_0}$

5.5.1.2 Frequency Response Tuning Rules

The tuning by using frequency response technique is an alternative way to set the controller parameters. It is necessary to develop the Bode plot for the TF. Table 7 show the tuning necessary to satisfy Ziegler-Nichols 4:1 ratio between first and second peak in the response. This criterion wish to achieve a certain damping in the response to a step reference [40, pp. 166]. It is very common to use this thumb rule in control system design, and this criterion is valid for the Ziegler-Nichols tuning, Zero-Pole-cancellation tuning, and Cohen-Coon tuning as well.

Table 7: Bode Plot Tuning parameters used for PID-regulators.

Tuning of regulator parameters				
	P	PI	PD	PID
$\angle G_P(j\omega_c$	Φ_m-180	Φ_m-160	Φ_m-220	Φ_m-200
T_i		$\frac{2.8}{\omega_c}$		$\frac{2.8}{\omega_c}$
T_d			$\frac{1}{\omega_c}$	$\frac{1}{\omega_c}$
$[K_R]_{dB}$	$-\lvert G_p(j\omega_c\rvert_{dB}$	$-\lvert G_p(j\omega_c\rvert_{dB}-1dB$	$-\lvert G_p(j\omega_c\rvert_{dB}-3dB$	$-\lvert G_p(j\omega_c\rvert_{dB}-4dB$

5.5.2 Prime Mover with PID Controller

The experimental step response of the prime mover is found by disconnecting the synchronous generator, and applying a step in rpm to the VFD and the induction machine. Running speed of the asynchronous machine is given as a 0-20 mA current signal by the VFD. A measurement bridge will be used in order to read the signal, using a 467.5 Ω resistor. The voltage over the resistor is measured by the

Picometer 4824. Figure 5.3 is the proposed block diagram for the experiment. The

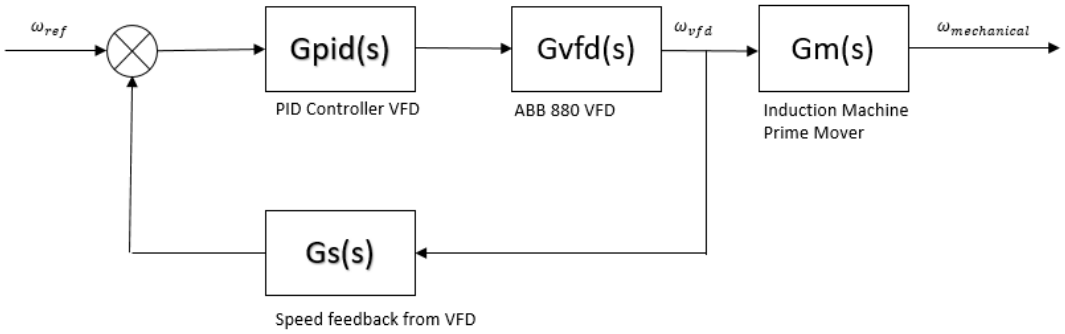

Figure 5.3: Blockdiagram for prime mover with PID control.

VFD will not have a feedback loop, it will calculate the speed using currents flowing to the induction motor.

5.6 Prime Mover and Generator with a Resistive Load

The generator will be loaded with a purely resistive load, the Terco MV1100 Load Resistor. The nominal level of active power, 1 kW, is chosen on the basis of the nameplate of the generator, see Table 2. Nominal voltage is selected to be 230 V. The field winding receives constant excitation current from the Langlois Compak40 ac/dc power supply. The step in mechanical speed will be given at different active loads, the experimental measure points is given in Table 8. Due to time limitations, the best measurement will be studied more thoroughly, and used in the coming tests.

Table 8: Experimental working points for dynamic response

$\frac{P}{P_n}$ [%]	0	20	60	80	90	95	100	105	110	120

5.6.1 Construction of the Transfer Function

The prime mover will be subjected to a step of 20 rpm in running speed, from 1500 rpm till 1520 rpm. Measurement with the oscilloscope is scheduled to be taken over 20 seconds, the step will be delivered at approximately 8 seconds. The prime

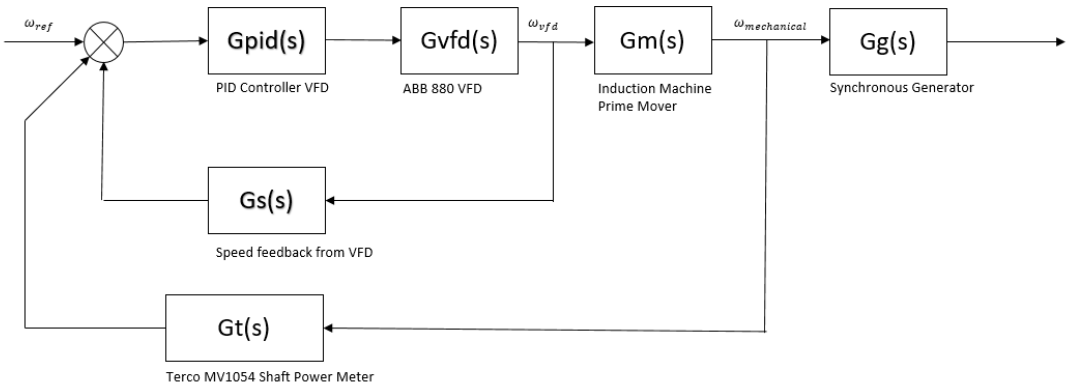

Figure 5.4: Blockdiagram for the system with controller and feedback loop.

mover and loaded generator is then given 12 seconds to stabilize at the new running speed.

The approximation will be adapted to the dynamic response with Equation (5.5). This is the general equation for first order TF in the time domain [21, pp. 166].

$$c(t) = a + b(1 - \exp(-t\,c)) \tag{5.5}$$

Where a is the mean steady-state speed prior to the step. b is the step in rpm, approximately 20 rpm is desired. c is a constant that is manipulated to fit the curve to the dynamic response. Noting that $1/a$ is the *time constant* of the system, the time it takes for the step response to rise to 63 % of its final value [21, pp. 166].

5.6.2 PID Tuning

With the approximation the Bode Plot will be plotted, hence PID controller parameters. The reaction curve will be used to find Cohen-Coon and Ziegler-Nichols parameters for the controller [40, pp. 166-169]. The method of how this is done has been described earlier in this section. Once parameters has been established, testing will commence.

5.6.3 Dynamic Response with Change in Resistive Load

The test will check the behavior of the PID controller, when a step in active load is applied on the synchronous generator. The generator will be connected to the prime mover, running at synchronous speed, with nominal voltage at the armature. The armature of the generator is wired in wye. A purely resistive load will be connected to the generator. A second resistive load will be separated from the circuit with a switch. The PID controller will then be engaged, fixed at synchronous speed. Measurement of speed, current, voltage and torque shall be captured with the Picometer 4824. A Hioki multimeter will be used to measure that armature voltage is at rated level. The Fluke Power Quality Analyzer observes currents and voltages. The switch is then flipped, and an additional load will be connected to the circuit. The response of five different controller settings will be captured and compared. A small dip in running speed is expected when the additional load is connected, the controller is then expected to increase the power output from the VFD, bringing the prime mover back to synchronous speed.

5.6.4 Stability Analysis with Root Locus

The Root Locus technique is used to reveal which gain that can be used in a closed loop system, without causing instability. This analysis will be performed on the prime mover and generator with a resistive load. The analysis involves two steps: (i) Sketching the root locus for the system TF, $G_m(s)$; (ii) Sketch the root locus for the PID controller, without including gain.

These two plots will reveal the critical gain for the system and controller. The controller and system will then be combined in a closed loop, and the critical gain will be included. A step will be applied, and the dynamic response of the system will be examined for stability. Fine-tuning of the parameters will be done, to narrow down an interval for which the system is stable.

5.7 Mechanical Machine Constants

The machine constants for the synchronous generator and induction machine prime mover will be calculated by evaluating the angular acceleration and torque during the step response. The calculations will result in the moment of inertia J and the inertia constant H. From this the mechanical starting time M can be calculated. These can be found by using Newton's Laws of Motion and the swing equation, as described by Kundur [2, pp. 128–131].

The synchronous generator will be open-circuited, and at synchronous speed. A step in speed will be applied. Mechanical torque and speed is measured with the Picometer 4824 through the Terco MV1054 Digital Torque, Speed and Shaft Power Meter. The torque, acceleration of the rotor, and running speed is needed to complete the calculations. The following Equations is used to calculate the machine constants.

$$J = \frac{T_M}{\dot{\omega}} \tag{5.6}$$

Where J is the moment of inertia in kgm^2, T_M is the mechanical torque needed to accelerate the machines in Nm, and $\dot{\omega}$ is the angular acceleration rad/s^2.

$$H = \frac{2 \times J \times \omega_{sm}}{VA} \tag{5.7}$$

Where H is the inertia constant in *seconds*, J is the moment of inertia, ω_{sm} is the rotor angular speed, and VA is the VA-base of the generator.

$$T_M = M = 2H \tag{5.8}$$

Where T_M is called the mechanical starting time.

5.8 Measurement in a Laboratory Environment

The measurements from the generator terminals were recorded with a Picometer 4824 digital oscilloscope. Voltages from the generator were fed through a differential probe to prevent harmful voltages on the terminals of the scope. Currents were measured with Fluke i5s AC current clamps, then fed into the scope. A Fluke Power Quality Analyzer was used to record currents and voltages in the OCC- and SSC-test. Two Hioki multimeters was also utilized. A Terco MV1054 Digital Torque, Speed and Shaft Power meter was installed between the synchronous machine and drive motor. The MV1054 uses a magnetically, contactless torque sensor to register speed and power on the shaft [41]. The MV1054 used in this thesis has an additional analog 0-10 V output for speed, which was used as a data input in the control loop.

5.8.1 Noise Reduction

All electric machinery produce harmonic noise. Most of the measurement equipment represent voltages and currents in millivolts or milliamperes in the signal processing software. Thus, when operating with such small figures, noise has an important impact on the result seen on oscilloscopes. An electronic drive was used to control the asynchronous prime mover, and by altering the frequencies to obtain the desired running speed, extensive amounts of harmonic noise is produced. Even in a laboratory environment, this can not be avoided. Thus, the measurement devices and wires were shielded from the generator and VFD. A grounded aluminum plate was placed between the machine rig and the measurement devices. All wires were wrapped in grounded aluminum foil. The wires that supplied the control signal to the drive were shielded from our instruments and all the way in to the terminal connections in the drive.

5.8.2 Filtering and Sample Rate

In the Picoscope software, a low pass filter was applied to the measurement data. Power system signals tend to have an low frequency, so filtering used 30-100 Hz

depending on which test that was performed. For tests regarding speed, the measurement signal is a dc voltage. When running tests on the terminal voltage, the measurement signals will be a 50 Hz ac voltage. In Matlab, a median filter was used, and averaging size depended on the sampling size chosen for the various tests. A median filter is an averaging filter, which is used to recover a repetitive measurement signal affected by noise [33, pp. 117]. This technique can be applied is cases where the signal RMS is much smaller than the noise.

A continuous signal, when measured, is represented by a set of samples taken at different time intervals [33, pp. 247]. It was attempted to match the duration of the phenomenas with the sample rate. The Picometer 4824 has a maximum sample rate of 1.000.000 samples for each window. By running tests at this sample rate, oversampling can be the result when examining the slower responses, such as a mechanical system. If a signal is oversampled, the distortion in the signal will become more prominent. Then, it may be difficult to separate the true signal from the noise. The sampling rate should comply with the Nyquist sampling theorem if the sampled signal is to be an accurate representation of the measured signal. The theorem is satisfied if the continuous signal is represented by a set of samples to which the number of samples per second is at least twice the highest frequency present in the signal [33, pp. 247]. The Nyquist theorem describes the minimum sampling rate, and is shown in Equation (5.9).

$$f_s \geq 2f_{max} \tag{5.9}$$

6 Result

The results from the modeling of the prime mover and synchronous machine is presented in this section. The electrical parameters of the synchronous generator have been calculated using tests. Different PID controllers have been designed and tested with and without the synchronous generator. The mechanical machine constants have been derived from the dynamic response of the combined system. Stability of the controller has been examined.

6.1 Open-Circuit and Short-Circuit Characteristics

It is preferable to express generator quantities in per unit values. In Table 9 the selected base values which is used to calculate the per unit values is given. In both the OCC and the SSC-test the average of phase voltages and currents is used to plot the desired curves. Base values are chosen by the user, and those parameters that are most convenient for the following calculations should be picked. For the open-circuit and sustained short-circuit test, the rated voltage and rated three-phase power is selected. Base values for current and impedance is calculated as such.

$$I_{base} = \frac{S_{base}}{\sqrt{3}V_{base}} \tag{6.1}$$

$$X_{base} = \frac{V_{base}^2}{I_{base}} \tag{6.2}$$

In Figure 6.1 X_d is calculated by evaluating the field current required to induce

Table 9: Base values for Terco MV1027-235 Synchronous Generator

S_{base}	V_{base}	I_{base}	X_{base}
1200 VA	230 V	3.01 A	44.1 Ohm

rated voltage on the air-gap line when open-circuited, and the field current needed to produce rated current when applying a solid three-phase short.

$$X_d = \frac{I_{f.ssc}}{I_{f.occ}}\ p.u. \times X_{base} = \frac{0.136}{0.201} \times 44.1 = 29.8\,\Omega \tag{6.3}$$

Table 10: Experimental data recorded during Open-Circuit and Sustained Short-Circuit test. The first five rows is the open-circuit test, the five last is the sustained short-circuit test.

V_a	V_b	V_c	$I_{f.occ}$	$V_{f.occ}$	I_a	I_b	I_c	$I_{f.ssc}$	$V_{f.ssc}$
0.52	0.52	0.51	0.00	0.00	4.39	4.39	4.37	0.60	77.23
23.44	23.42	23.43	0.07	9.24	3.52	3.52	3.51	0.48	62.17
46.71	46.67	46.69	0.13	16.60	2.61	2.51	2.60	0.35	45.87
69.80	69.75	69.79	0.19	24.18	1.80	1.81	1.80	0.24	31.47
91.93	91.93	91.99	0.25	31.56	0.91	0.91	0.91	0.12	15.47
114.82	114.75	114.75	0.30	39.10	0.00	0.00	0.00	0.00	0.00
126.90	126.80	126.90	0.34	43.29					
138.50	138.40	138.50	0.37	47.50					
150.50	150.50	150.60	0.40	52.08					
159.60	159.60	159.70	0.43	56.28					
174.30	174.20	174.30	0.47	62.26					
183.90	183.90	183.90	0.50	66.40					
195.90	195.90	195.90	0.53	71.67					
206.30	206.10	206.20	0.57	77.34					
218.40	218.22	218.20	0.61	83.63					
230.90	230.70	230.60	0.65	90.37					
240.80	240.60	240.70	0.69	96.77					
253.60	253.30	253.30	0.74	104.89					
277.30	277.00	276.80	0.85	122.21					

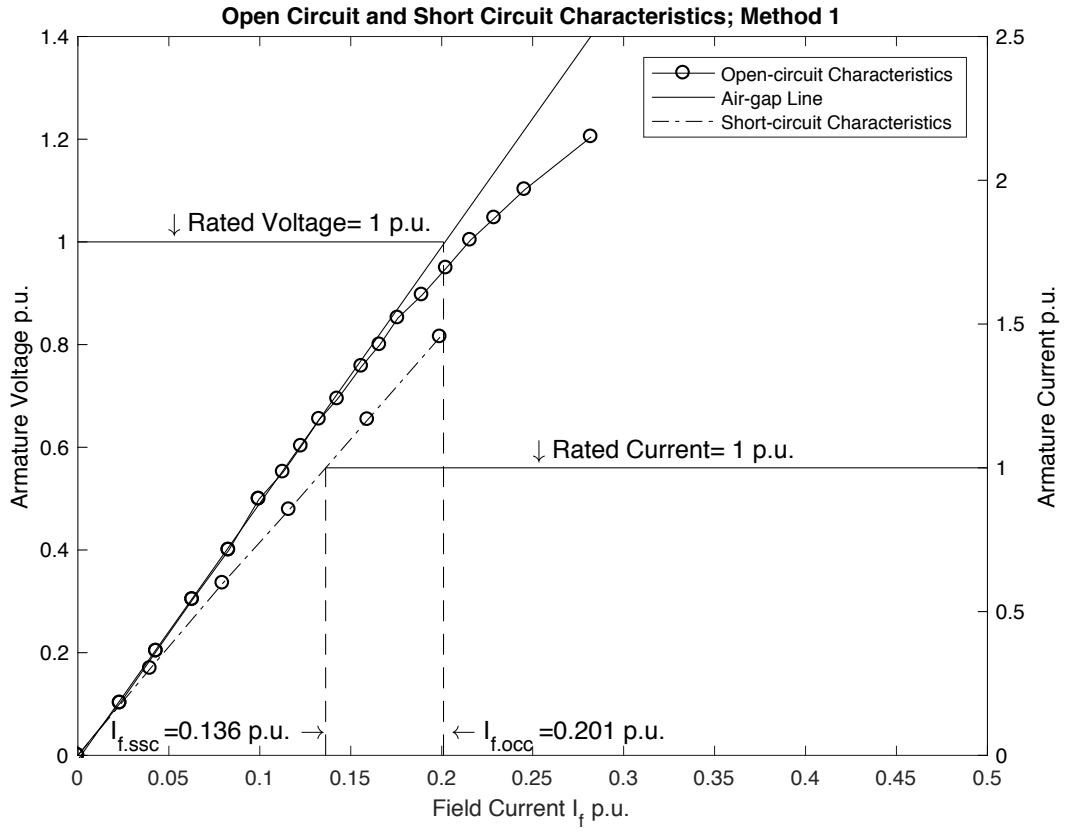

Figure 6.1: Open-Circuit and Short-Circuit Characteristics for Terco MV1027-235 Synchronous generator, using method 1. The dotted points indicate the values found during the tests.

The method applied in Figure 6.2 utilizes a field current freely selected by the operator of the test. In this test the field current selected by the author was 0.15 p.u. The values of terminal voltage on the air-gap line in the OCC-test, and the terminal current in the SSC-test is noted.

$$X_{d,p.u.} = \frac{V_{average}}{I_{average}}\ p.u. = \frac{0.74}{1.1} \times 44.1 = 29.7\ \Omega \tag{6.4}$$

Both methods using the OCC and SSC curves yield the same result. The OCC and SSC is familiar tests for most engineers devoted to electric power engineering. The results found from these test are reliable, and it is good reason to believe that the direct axis reactance is in the range of 29 ohms.

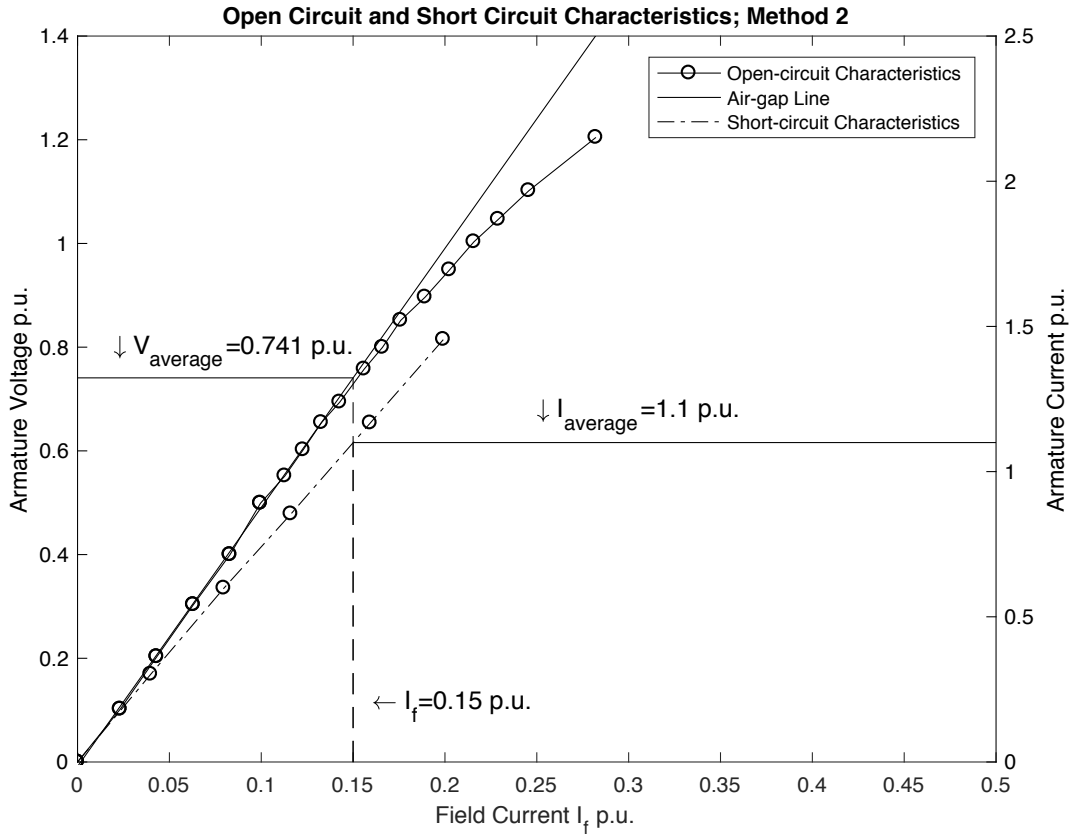

Figure 6.2: Open-Circuit and Short-Circuit Characteristics for Terco MV1027-235 Synchronous generator, using method 2. The dotted points indicate the values found during the tests.

6.2 Potier Reactance

The Potier reactance for the Terco Synchronous generator was found by constructing the Potier triangle between the OCC-curve and the ZPFC-curve. The Potier reactance is calculated using phase values of the voltage, and the rated current. The Potier triangle in Figure 6.4 gives the values required to complete the calculation.

$$X_P = \frac{238.7V - 230V}{\sqrt{3} \times 3.05A} = 1.65\,\Omega \tag{6.5}$$

In Section 6.1 the synchronous reactance for the machine is found to be 28.9 Ω.

$$X_P\% = \frac{1.65\Omega}{28.9\Omega} \times 100\% = 5.74\,\% \tag{6.6}$$

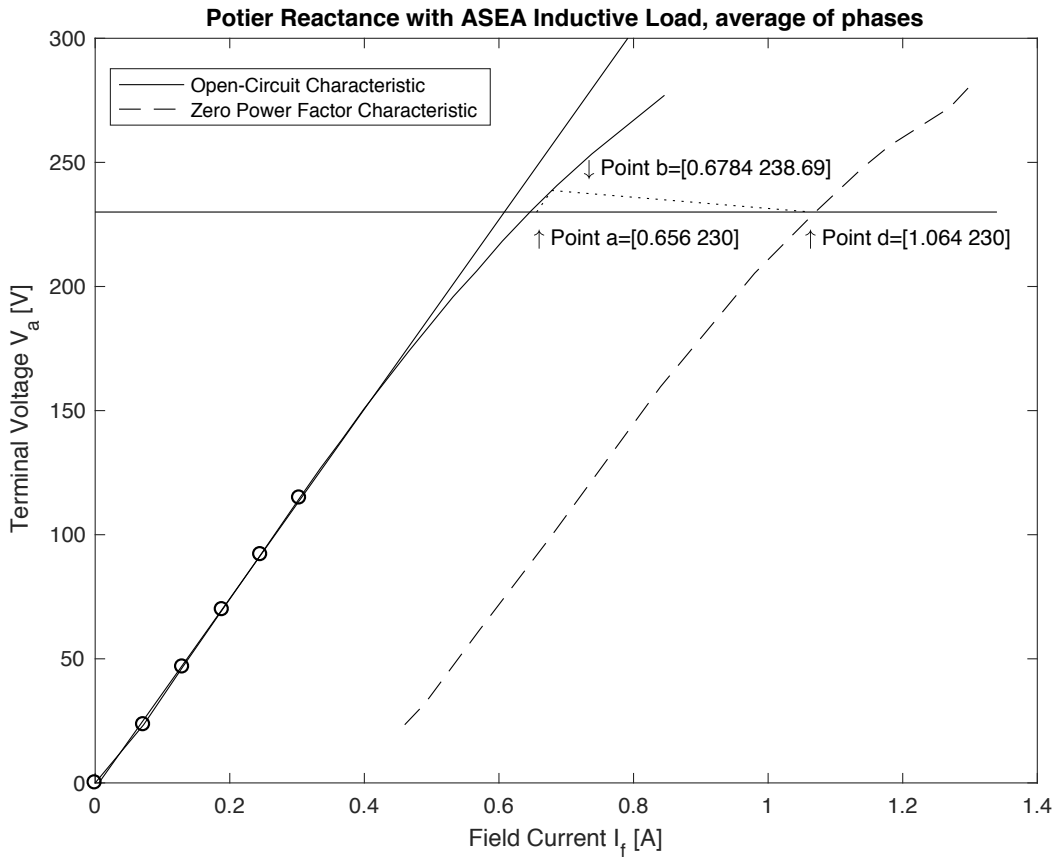

Figure 6.3: Plot showing the OCC and ZPFC curves, the Potier triangle is plotted with the dotted line.

Equation (6.6) show that the Potier reactance is in the range of 5 % of the synchronous reactance. As noted in literature [30–32], the Potier reactance can be as much as 100 % higher than the leakage reactance. From theory it is also known that the stator leakage reactance can be in the range of 10 % of the synchronous reactance [14, pp. 36]. This experiment was conducted at rated values, which usually is to low to get a correct result for the stator leakage reactance. However, the result is useful in understanding the value range in which the stator leakage reactance exists for the MV1027-235 synchronous machine.

It was attempted to perform an alternative test to achieve a more accurate representation of the leakage reactance. A more accurate method of calculating the leakage reactance is described [30]. This method require the synchronous generator operating unloaded and unexcited, and it is supplying a purely inductive source. When the author attempted to record the stator voltage/current characteristics with the

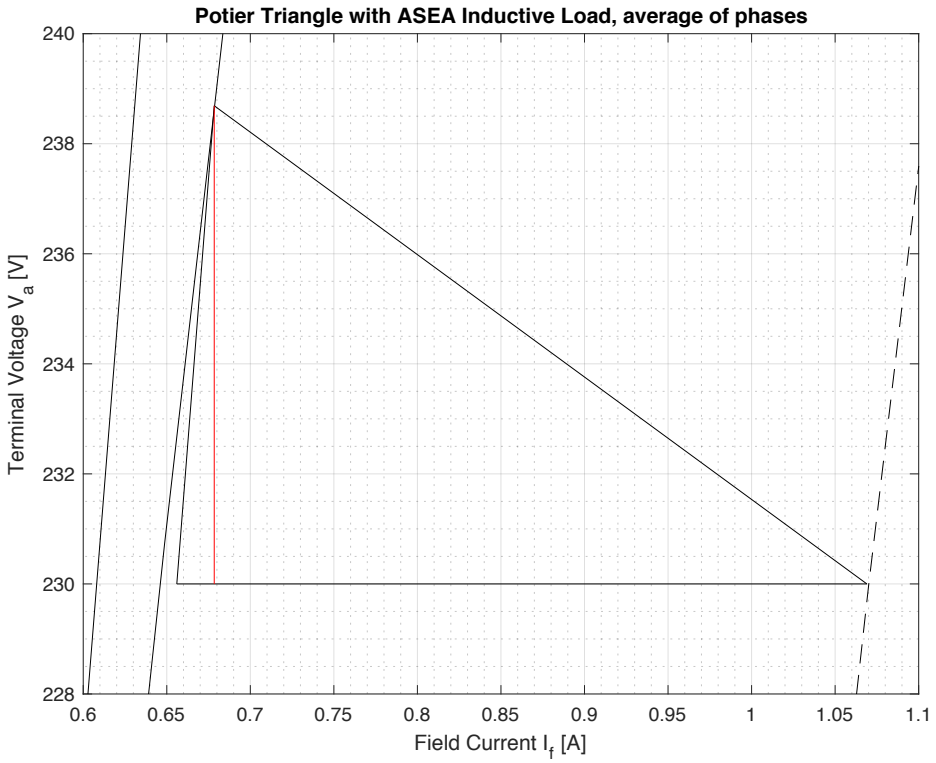

Figure 6.4: Enhanced picture of the Potier triangle.

synchronous machine unloaded and unexcited, it was not possible to reach rated speed. The machine was able to run at 750 rpm with no excitation. It was not possible to produce a result because of this. The experiment was then ended.

6.3 Slip Test

The results from the slip test were filtered in the Picoscope software, with a 1kHz filter, before being processed in Matlab. Figure 6.5 illustrates how the magnitude of the armature voltage and armature current oscillates as the field slips past the poles. Figure 6.6 shows the highly distorted field voltage induced in the field winding during the test, as well as separate plots of armature voltage and armature current.

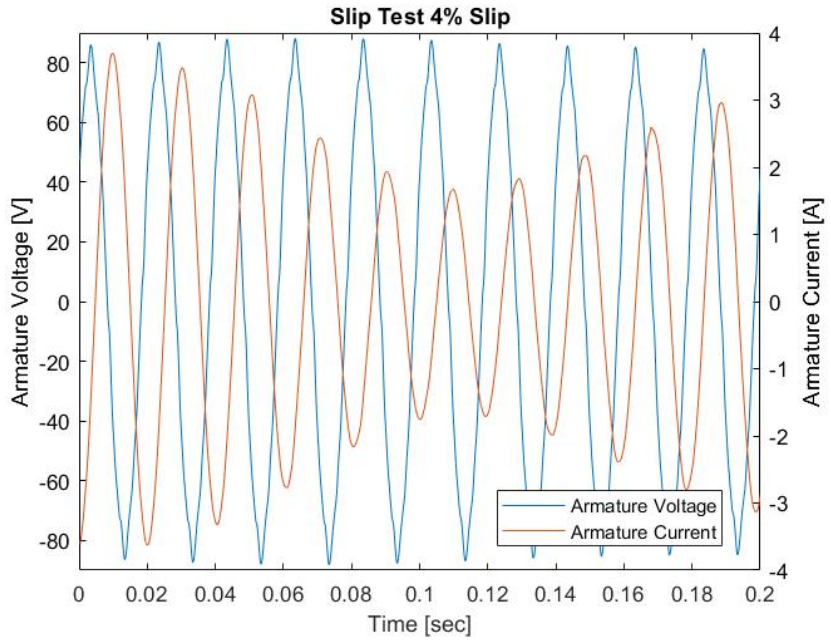

Figure 6.5: Plot taken from Matlab, showing the result of the slip test. The synchronous generator is subjected to a 4 % slip from synchronous speed.

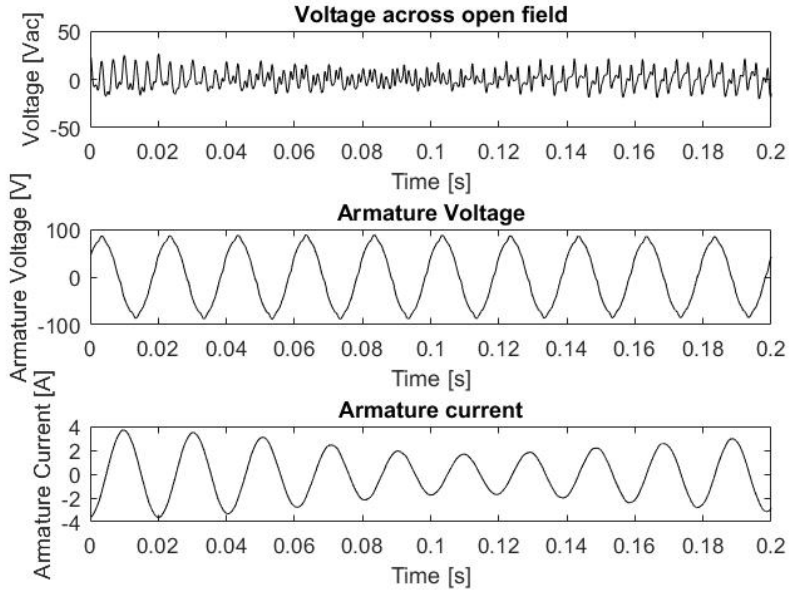

Figure 6.6: Plot showing voltage from armature and the field winding, and the armature current when running the generator at 4 % slip.

The local maximum and minimum points on both the armature voltage and current envelope curve was examined, and values penned down. Measurement was conducted on line voltage, in the following calculations this voltage is converted

to phase voltage.

$$V_{ab,max} = 88.22\ V$$
$$V_{ab,min} = 84.35\ V$$
$$I_{a,max} = 3.66\ A$$
$$I_{a,min} = 1.67\ A$$

$$X_{q,st} = \frac{V_{ab,min}}{I_{a,max}} = \frac{84.35V}{\sqrt{3} \times 3.66A} = 13.3\ \Omega \tag{6.7}$$

$$X_{d,st} = \frac{V_{ab,max}}{I_{a,min}} = \frac{88.22V}{\sqrt{3} \times 1.67A} = 30.49\ \Omega \tag{6.8}$$

The results presented in Equations (6.7) and (6.8) corresponds with values for the direct axis synchronous reactance found experimentally in Section 6.1. The slip test was an unfamiliar test for the author, but it proved quit manageable to execute. Different values of slip was tested, and it was an interesting study to observe the behavior of the synchronous generator when it was subjected to a large slip. It was audible when the machine slipped past the poles, and it could be seen on the MV1054 that the speed of the machine pulsated at higher slips. Care was taken not to induce harmful levels of voltage in the machine.

6.4 Prime Mover Experimental Step Response

The goal of this section is to find the transfer function of the mechanical system through an experimental step response test. As most systems need a controller system to maintain synchronous speed, which is vital to stable power production, experiments were made with different controllers. Due to a lack of time, the main study is the PID-controller. Several different controller settings have been tested, and they have been found by following different tuning rules, such as the 4:1 ratio proposed by Ziegler and Nichols and peers [20].

6.4.1 Prime Mover with PID Controller

Figure 6.7 shows the dynamic response of the prime mover, and the approximation, i.e. the first order TF with delay used to model the behavior of the system. Equation (6.9) is the approximation in time. Equation (6.13) is the TF for the induction prime mover in closed-loop.

$$g(t) = a + b(1 - exp(-t/T)) \tag{6.9}$$

$$a = 1490\,[rpm] \tag{6.10}$$

$$b = 20\,[rpm] \tag{6.11}$$

$$T = 0.58\,[sec] \tag{6.12}$$

Where a is the initial speed, b is the step in rpm and T is the experimental time constant.

$$G_{CL} = \frac{(1 - 0.0805s)}{\frac{0.00187s^2}{k_R} + \left(\frac{0.023}{k_R} - 0.0805\right)s + 1} \tag{6.13}$$

By using mean value of steady-state rpm before the step, the approximation became a good fit for the dynamic response of the system. This response was used to tune a PID controller, to properly regulate running speed at synchronous speed, 1500 rpm. For the prime mover, a number of settings for the PID controller is available from multiple methods of tuning. Most methods rely on the reaction curve of the process. In Table 11 the different controller settings are presented. The

Table 11: PID Tuning parameters for the prime mover

	k_R	T_i	T_d
Zero-Pole-Canceling [PI]	0.142	0.512	
Bode Plot	0.146	0.29	0.103
Cohen-Coon Tuning	0.287	0.475	0.058
Ziegler-Nichols Tuning	0.248	0.334	0.0835

VFD was then put in rpm-mode, and the PID-controller was activated. Tuning parameters from Table 11 was set, and the response of the system when subjected to a 20 rpm step is shown in Figures 6.9, 6.10, 6.11 and 6.12. The Ziegler-Nichols tuning showed the best response of the different tunings. It had a quick rise time,

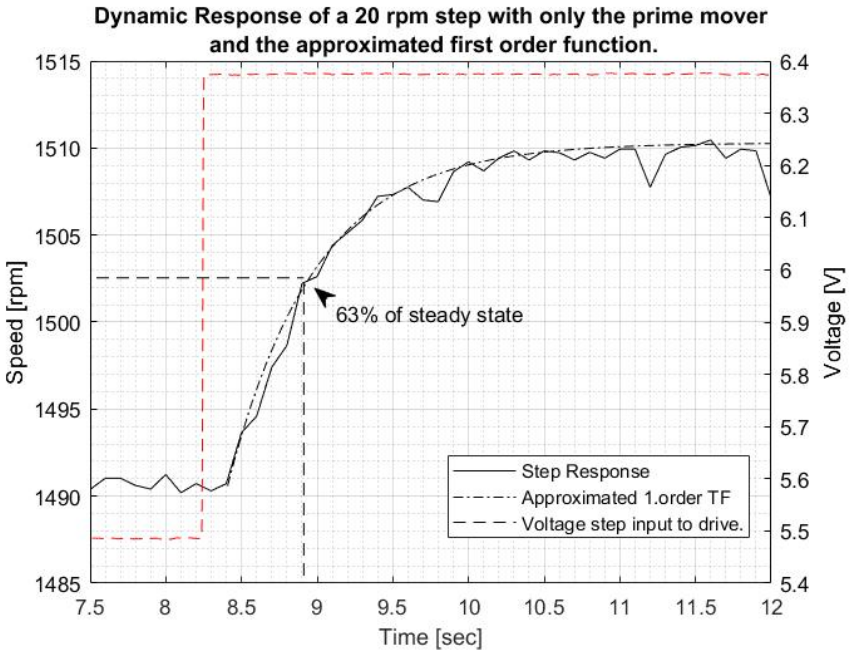

Figure 6.7: The dynamic response of the prime mover element when subjected to a step of 20 rpm. The approximation is plotted, together with the step input.

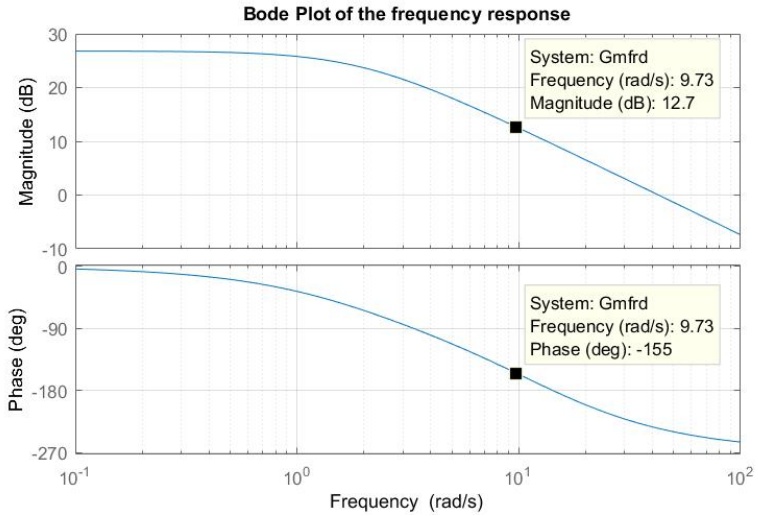

Figure 6.8: The Bode plot for the prime mover, showing the frequency response for the process. This plot is used to tune the PID controller.

and reached steady state rapidly. The zero-pole-cancellation showed the poorest qualities, i.e the longest rise time. The Cohen-Coon shows similar qualities as the Ziegler-Nichols tuning. Tuning the PID using a frequency response technique results in a higher overshoot in the first peak.

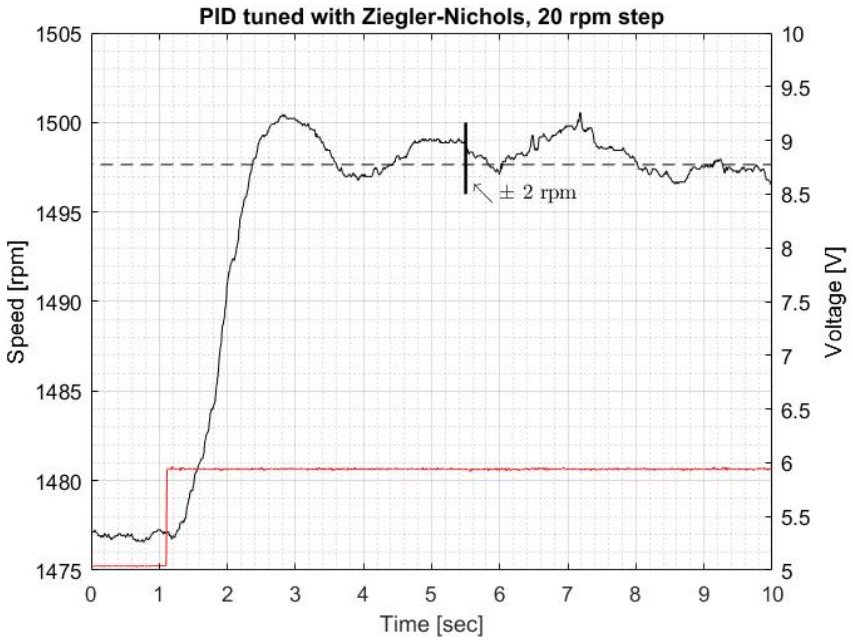

Figure 6.9: The dynamic response with a controller. The PID is tuned with Ziegler-Nichols tuning rules. The bar in the plot indicate how much the response deviates from the calculated mean.

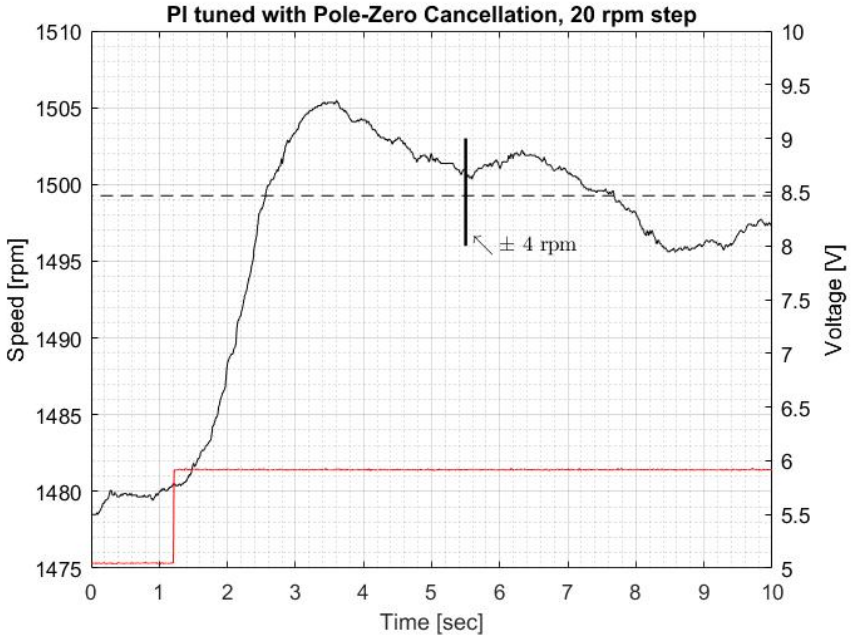

Figure 6.10: The dynamic response with a controller. The PID is tuned with Pole-Zero cancellation. The bar in the plot indicate how much the response deviates from the calculated mean.

From mean value of the steady-state value, all PID-controllers would adjust the running speed, so that the speed revolves around ± 2 rpm. This is a frequency

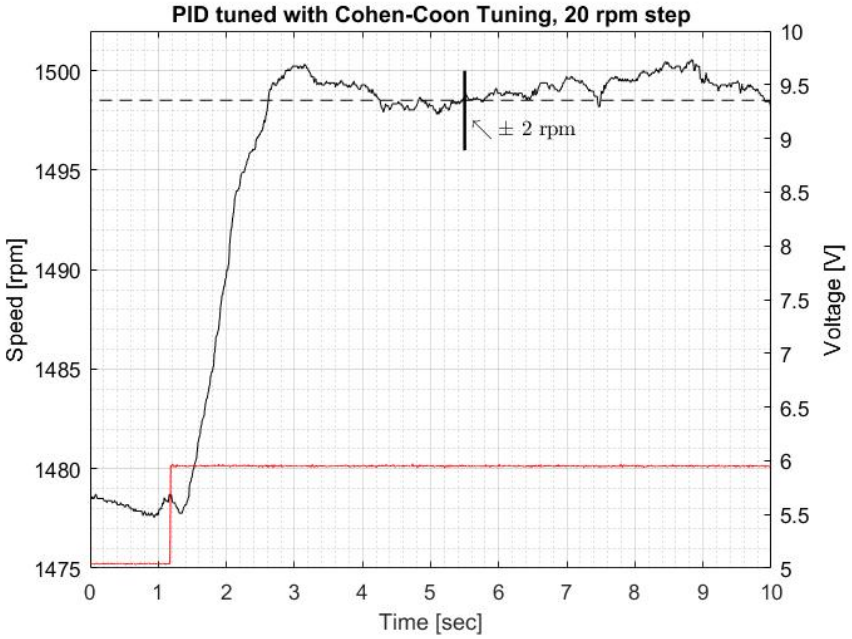

Figure 6.11: The dynamic response with a controller. The PID is tuned with Cohen-Coon tuning rules. The bar in the plot indicate how much the response deviates from the calculated mean.

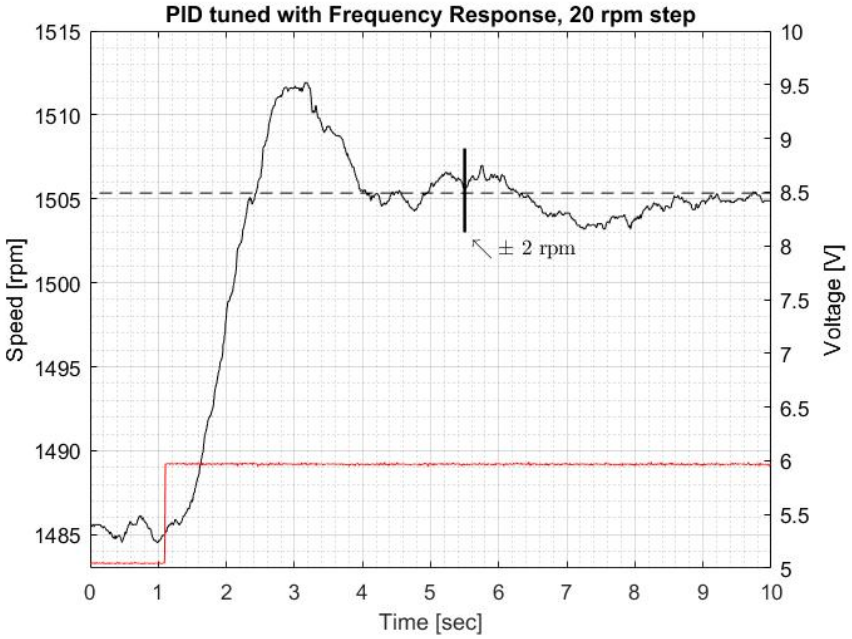

Figure 6.12: The dynamic response with a controller. The PID is tuned with the frequency response technique. The bar in the plot indicate how much the response deviates from the calculated mean.

deviation of 0.067 Hz when operating at synchronous speed. This indicates stability [21, pp. 303].

The tests applied on the prime mover alone were performed in open loop system, i.e. without feedback. The calculated running speed from the drive was used to create plots, tune the controller and so on. Extensive works has been put into understanding the VFD. There is several PID controllers that adjust the output. In addition, there may be some stabilizing loops as well. When setting PID parameters, the gain, integration time and derivation time, the drive controller lacked the resolution to set the calculated PID parameters. This challenge was solved by rounding the calculated parameters to the closest available figure in the VFD, this worked very well.

6.5 Prime Mover and Generator with a Resistive Load

This section show the result when a step was given to the system with a loaded generator. The approximated function is created. Results from this test has been used to calculate machine constants, applicable to rated loading for the generator.

The generator was loaded with a purely resistive load of 1050 W. A number of measurement points were acquired. The measurement at 1050 W was the most "clean" data series registered, and on the basis of this its processing was pursued. Equation (6.14) is the transfer function for the combined system of drive, induction machine and synchronous generator with load.

$$G_m(s) = \frac{28.16 \times (1 - 0.58s)}{0.016s^3 + 0.25s^2 + 0.96s + 1} \tag{6.14}$$

The step response was used to derive the transfer function for the system. The derivative of the system response was used to determine when the step started. Figure 6.13 shows a plot of the derivative and the system response. The step occurs after 9.3 seconds. The step to the VFD was given at 8.14 seconds, this is seen in Figure 6.15. The output response starts at 9.4 seconds. At 9.68 seconds, the system reaches 63 % of the final, steady-state value, defining the time constant. The delay between the step into the VFD, and the time it takes the output to begin to change is the time delay τ. All time constants and delays are given in Table 12.

Table 12: Experimental time constants

τ	T_1	T_2
1.16	0.1	0.27

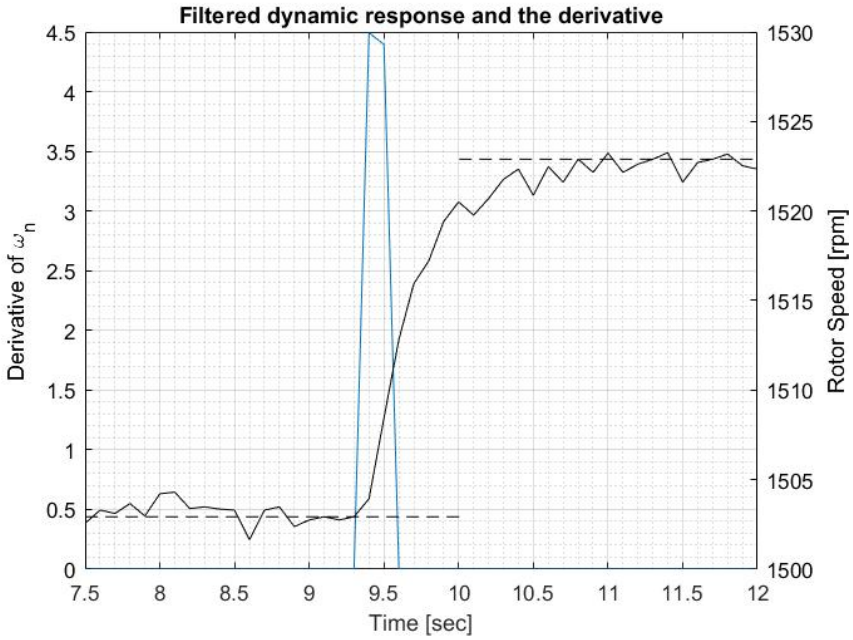

Figure 6.13: The derivative of the system response plotted against the actual response. This curve shows where step is applied.

6.5.1 PID Tuning

The Ziegler-Nichols tuning and Cohen-Coon tuning relies on the reaction curve of the dynamic response. It is adequate to observe the dynamic response graphically in order to draw the reaction curve. The frequency response tuning is derived from the Bode plot of the closed-loop transfer function.

6.5.1.1 Reaction Curve Tuning Technique

The reaction curve of the loaded generator and prime mover is drawn in Figure 6.14. The tangent is drawn on the steepest point on the reaction curve. The three points of interest are found: (i) the point where the tangent crosses the final steady-state value of the response, $t_2 = 9.86$ seconds; (ii) the point where the tangent crosses

the pre-step steady-state value, $t_1 = 9.35$ seconds; and (iii) the starting time of the step input, $t_0 = 8.14$ seconds.

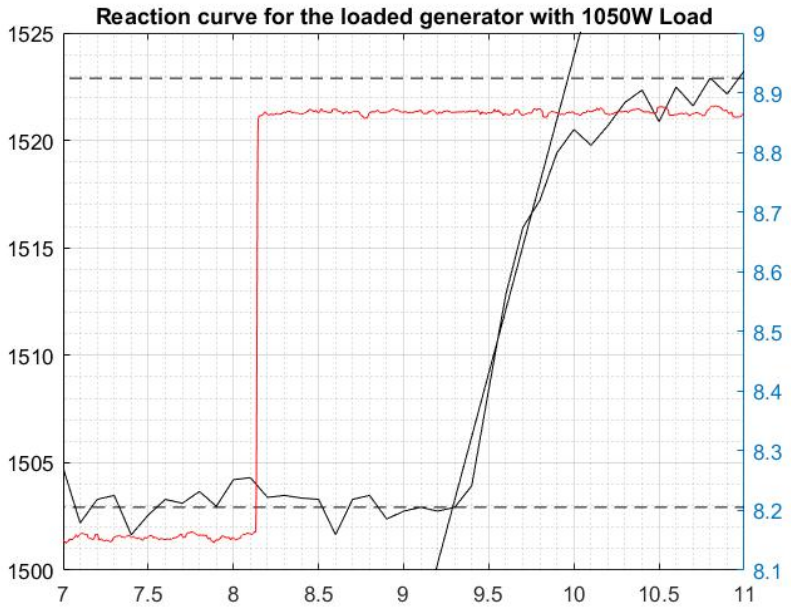

Figure 6.14: The reaction curve for the loaded generator.The input step to the VFD is shown. The tangent is drawn in the most steep point on the response curve.

Using the formulas and tuning rules from Section 5.5.1.1, the Ziegler-Nichols and Cohen-Coon PID parameters is calculated.

6.5.1.2 Frequency Response Tuning Technique

To use the frequency response tuning technique, the transfer function for the system was needed. The approximation of the step response was a first order response, for the plots given in the thesis Equation (6.15) was used.

$$c_m(t) = a + \left(b \left(1 - \exp \frac{-t}{T} \right) \right) \tag{6.15}$$

$$a = 1503\,[rpm] \tag{6.16}$$

$$b = 19.5\,[rpm] \tag{6.17}$$

$$T = 0.265\,[sec] \tag{6.18}$$

Where a is the speed prior to the step. b is the step in rpm. T is the experimental time constant of the fitted curve. After determining the gain k_m and using the time

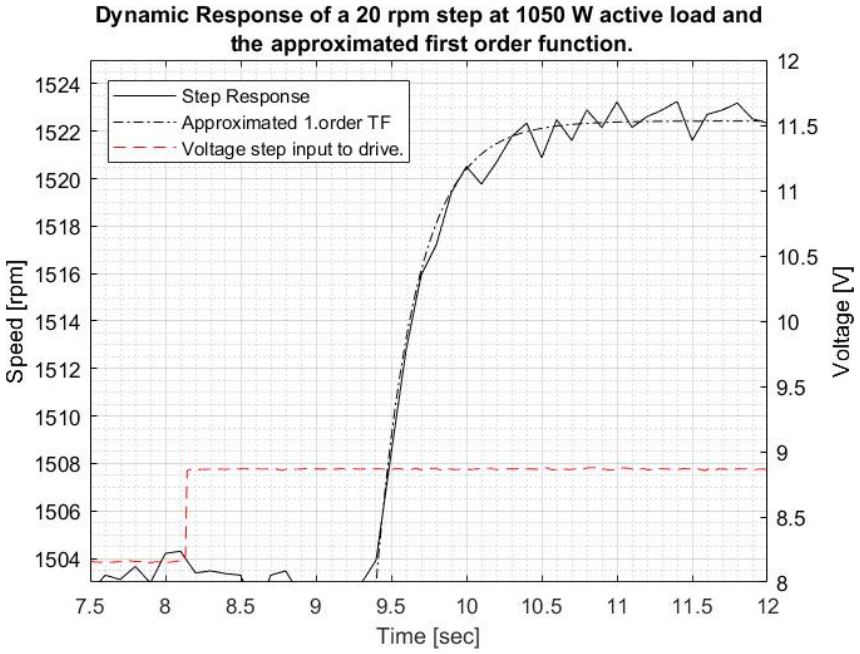

Figure 6.15: Plot showing the actual response versus the approximated 1. order system response.

constants, the TF for the process could be obtained.

$$k_m = \frac{\Delta\omega}{\Delta V} = \frac{1523rpm - 1503rpm}{8.86V - 8.5V} = 28.16\left[\frac{rpm}{V}\right] \tag{6.19}$$

The delay was transferred to polynomial form by the use of the 1. order Padé-approximation [21, pp. 334].

$$G_m(s) = \frac{28.16rpm/V(1-0.58s)}{(0.1s+1)(0.27s+1)(0.58s+1)} \tag{6.20}$$

The tuning of the PID could then commence. A response of the minimum area type was desired. The stability limits that needed to be fulfilled were $G_m > 12dB$ and $\Phi_m > 45°$. The calculations was performed using the values from Table 7 and Figure 6.16. The Bode plot for the figure was created with the system in open loop, with the regulator included. Figure 6.16 was used to tune the various parameters of the PID for the prime mover.

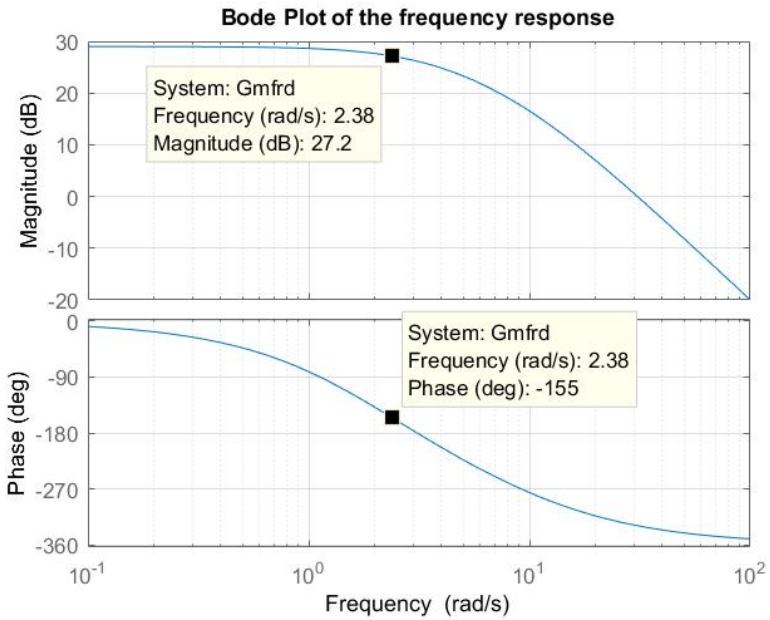

Figure 6.16: Bode plot used to tune the PID regulator for the prime mover.

$$\angle G_m = -155° \tag{6.21}$$

$$\omega_c = 2.38 rad/s \tag{6.22}$$

$$|G_M|_{db} = 27.2 dB \tag{6.23}$$

$$T_i = 1.17 s \tag{6.24}$$

$$T_d = 0.42 s \tag{6.25}$$

$$k_R = 0.043 \tag{6.26}$$

6.5.1.3 Tuning Parameters

The calculated tuning parameters are presented in Table 13. The Cohen-Coon tuning parameters were selected for the PID for the next experiment, where a step in load was given. The Cohen-Coon tuning had parameter values that were in be-

Table 13: PID Tuning parameters for the loaded generator, calculated.

	k_R	T_i	T_d
Frequency Response	0.043	1.17	0.42
Cohen-Coon Tuning	0.03	1.75	0.308
Ziegler-Nichols Tuning	0.017	2.424	0.606

tween the Frequency Response- and Ziegler-Nichols tunings. The values calculated by the Cohen-Coon method can be used to fine-tune the PID further if needed.

6.5.2 Dynamic Response with Change in Resistive Load

In this experiment two resistive loads were connected to the synchronous generator. The Terco MV1100 Resistive Load was drawing 1000 W at 230 V from the generator. Another resistive load was separated from the circuit by a three-pole switch. The generator speed was controlled by the VFD, and running at synchronous speed. At a given time the switch was turned, applying additional loading of 190 W to the generator. The system response was captured, and is shown in Figure 6.17.

In Table 13 the calculated settings for the controller are given. The Cohen-Coon setting were used further in the following experiment. Table 14 shows different experimental settings for the controller used in the test. The first was the default setting for the VFD in Direct Torque Control (DTC) mode. The second setting was calculated using the tuning rules of Cohen-Coon. The gain, k_R, was set to 0.1, the lowest value the controller of the VFD could be adjusted to in DTC mode. When this response was tested, the PID was adjusted freely, to examine different responses to different controller settings. Figures 6.17 and 6.18 shows the system response

Table 14: PID Tuning parameters for loaded generator, experimental.

	k_R	T_i	T_d
Internal PI	5	5	
Experimental PID 1.	0.1	1.7	0.303
Experimental PID 2.	0.6	1.7	0.303
Experimental PID 3.	3	1.7	0.303
Experimental PID 3.	3	1.7	0.6

to a change in load. The goal is to maintain the predefined frequency as close to 1500 rpm as possible, while the system undergoes a change. The initial, calculated Cohen-Coon tuning gave the most rapid controller response with minimum overshoot and few oscillations. The controller responded faster to the speed deviation than in the other cases, and brought the speed back to rated. This can be seen in Figure 6.19. When the load was connected, the speed dropped with 30 rpm from

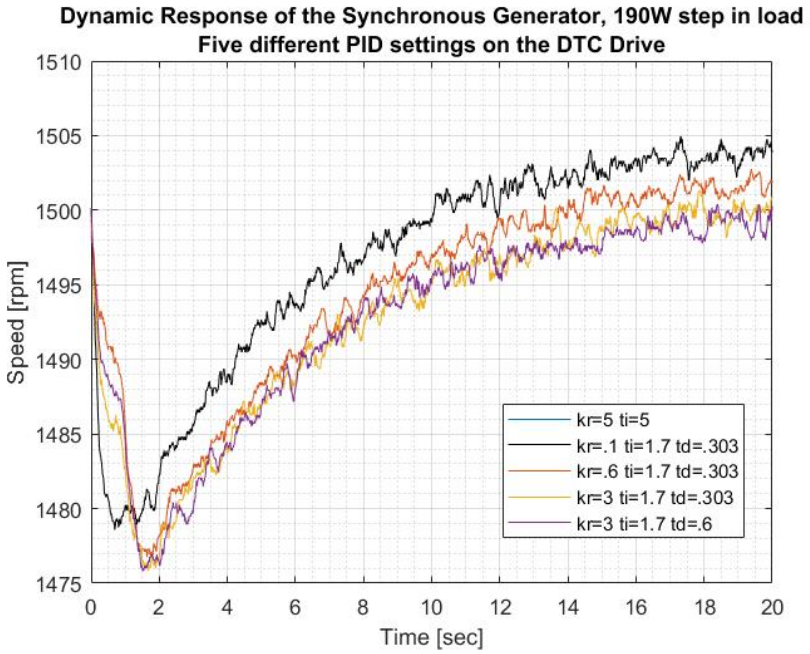

Figure 6.17: Response of the PID when an increment in active, real load is applied on the synchronous generator. Controller settings from Table 14 is used.

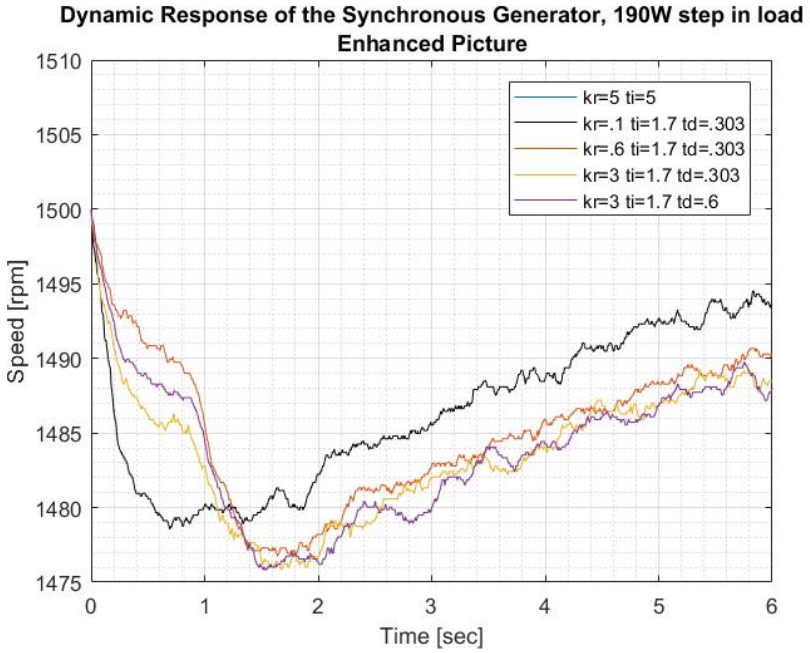

Figure 6.18: An enhanced picture of the system response from Figure 6.17.

synchronous speed, a total of 2%.

$$f = \frac{4}{2} \times \frac{30}{60} = 1\,[Hz] \tag{6.27}$$

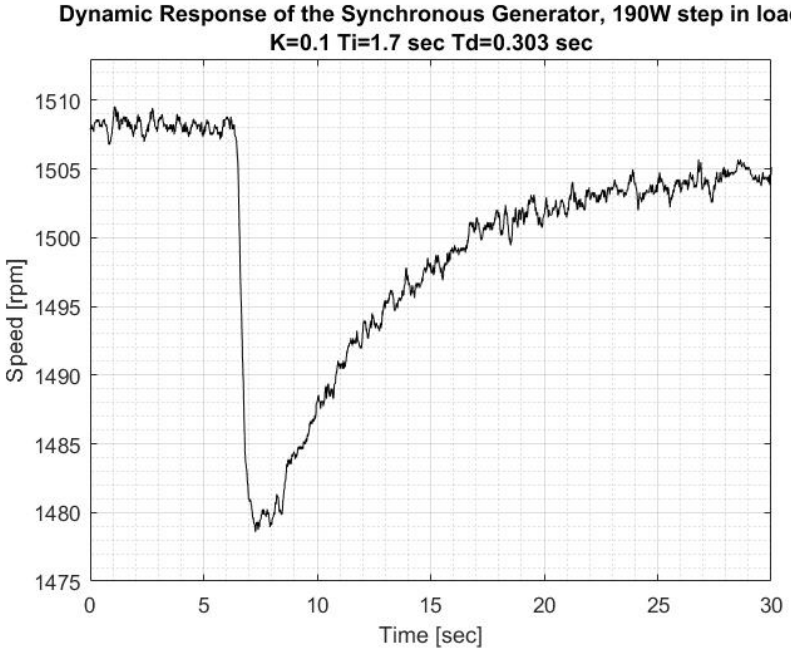

Figure 6.19: The system response when Cohen-Coon tuning of the PID controller was used. This setting showed the best response.

This additional loading resulted in a frequency drop of 1 Hz. For brief periods of time, this is within the limits given in Std. En 50160 [4]. For a single generator, operating as an "island", this frequency deviation is within limits given by legislation [42, §3-2]. In a real, multi-machine scenario, the power system would keep the frequency at synchronous level, due to the *stiff* nature of the interconnection.

6.5.3 Stability Analysis with Root Locus

A stability analysis has been performed on the loaded generator. The Root Locus reveals which gain can be applied to the system without causing instability. The crossing of poles from left half-plane to right indicates that the system is unstable [21, pp. 405].

The root locus is sketched for the controller and system respectively, the TF of both systems is given in Equations (6.28) and (6.29). The measurement used to construct these TFs was with 1000 W purely resistive load, the generator operating at rated

conditions, and in a wye-connection.

$$G_m(s) = \frac{21.11s^2 - 745.2s + 8767}{0.89s^3 + 32.41s^2 + 404.8s + 415.2} \tag{6.28}$$

$$G_{PID}(s) = \frac{0.5151s^2 + 2.003s + 1}{0.05151s^2 + 1.7s} \tag{6.29}$$

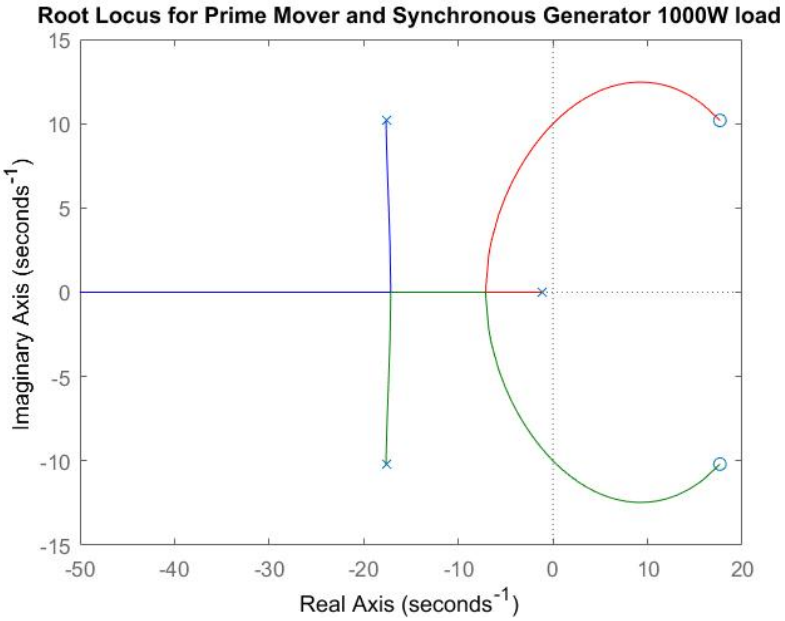

Figure 6.20: The Root Locus of the closed-loop system with a load of 1000 W. The plot shows the location of the system poles.

The root locus is sketched in Figure 6.20, and is used to examine stability properties for the system without controller. The points on the real axis where the root locus enters or leaves the complex plane are points of interest, that gives the critical gain needed to maintain stability and such [21, pp. 402]. Examining the locus, a gain larger than 0.1 will cause instability, the poles are then located in the right half-plane.

Next, the root locus of the Cohen-Coon PID is examined. The gain is not included, only T_i and T_d.

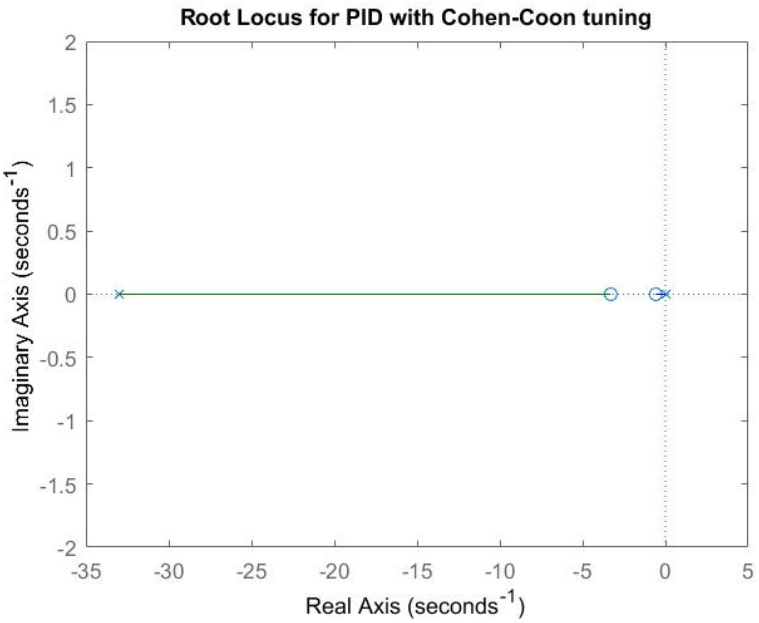

Figure 6.21: The Root Locus of the Cohen-Coon PID Controller. $T_i = 1.7$, $T_d = 0.303$ The plot shows the location of the system poles.

The PID controller will not enter the right half-plan for any value of gain, as seen in Figure 6.21. The highest gain found on the root locus is 11.3.

The testing commenced by closing the loop with controller and system, then experimentally test the dynamic response for different gains. The interval for the gain is presented in Equation (6.30). The system response is plotted in Figures 6.22 and 6.23.

$$k_R > 12.9 \vee k_R < 0.1 \tag{6.30}$$

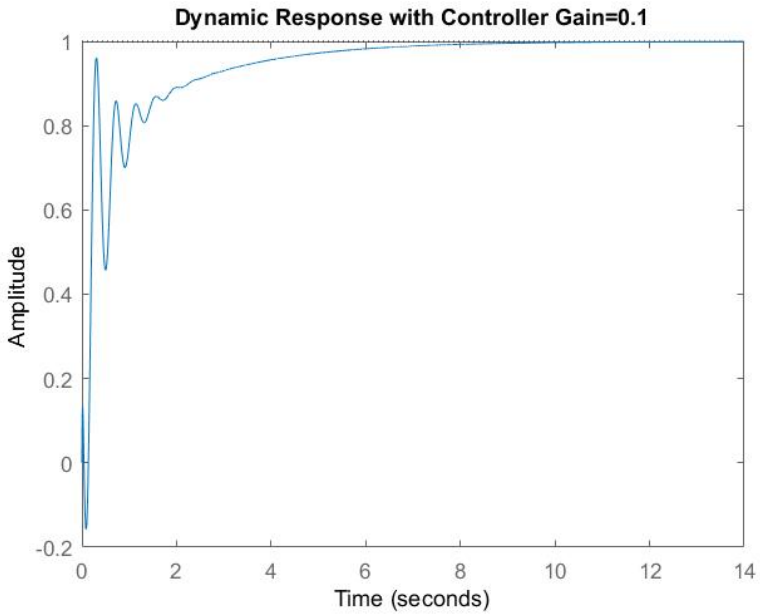

Figure 6.22: Dynamic response of closed loop system with controller gain 0.1. If gain is increased, the system becomes gradually more unstable.

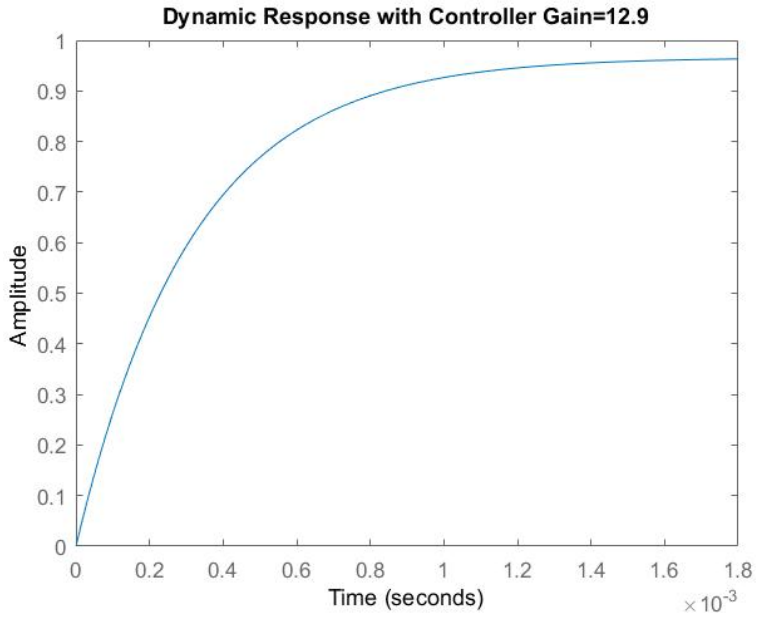

Figure 6.23: Dynamic response of closed loop system with controller gain 12.9. If gain is decreased, the system becomes gradually more unstable.

The experiments from the previous section has shown that it was possible to use gain higher than 0.1. The stability test performed is a theoretical approach, and

fine-tuning of the controller around the theoretical setting is always done. When using the VFD there are more than one PID active. There is one PID which uses the calculated mechanical speed to control output speed. In DTC mode, another PID is introduced with a feedback signal of the mechanical speed from the Terco MV1054. The complex nature of the VFD may participate in keeping the system stable outside boundaries found in Equation (6.30).

6.6 Mechanical Machine Constants

Main machine constants of interest are the moment of inertia J and the inertia constant H. The machine constants found for unloaded generator, and with 1000 W rated load. The constants include the synchronous generator, induction prime mover, and the MV1054 Digital Torque, Speed and Shaft Power Meter. The machine constants can be used to model the mechanical system of the generator. This is necessary if a complete power control system will be designed, with voltage and frequency regulation.

6.6.1 No Load Machine Constants

For the unloaded machine it is possible to find the combined moment of inertia of prime mover and synchronous generator, as well as the inertia constant.

Figures 6.24 and 6.25 is plots of the mechanical torque and mechanical speed of the system during the step response. Values from these plots are used to derive the no-load machine constants.

$$T_{mean.upper} = 0.956\,[Nm] \tag{6.31}$$

$$T_{mean.lower} = 0.944\,[Nm] \tag{6.32}$$

$$\Delta t = 11.92 - 8.358 = 3.56\,[sec] \tag{6.33}$$

$$\omega_{mean.upper} = 159.5\,[rad/s] \tag{6.34}$$

$$\omega_{mean.lower} = 157.4\,[rad/s] \tag{6.35}$$

$$\dot{\omega} = \frac{159.5 - 157.4}{3.56} = 0.59\,[rad/s^2] \tag{6.36}$$

$$J = \frac{0.956 - 0.944}{0.59} = 0.0204\,[kgm^2] \tag{6.37}$$

$$H = \frac{1}{2} \times \frac{0.0204 \times (157.08)^2}{1200} = 0.2\,[sec] \tag{6.38}$$

$$T_M = 0.4\,[sec] \tag{6.39}$$

The combined moment of inertia is within range of the nominal moment of inertia,

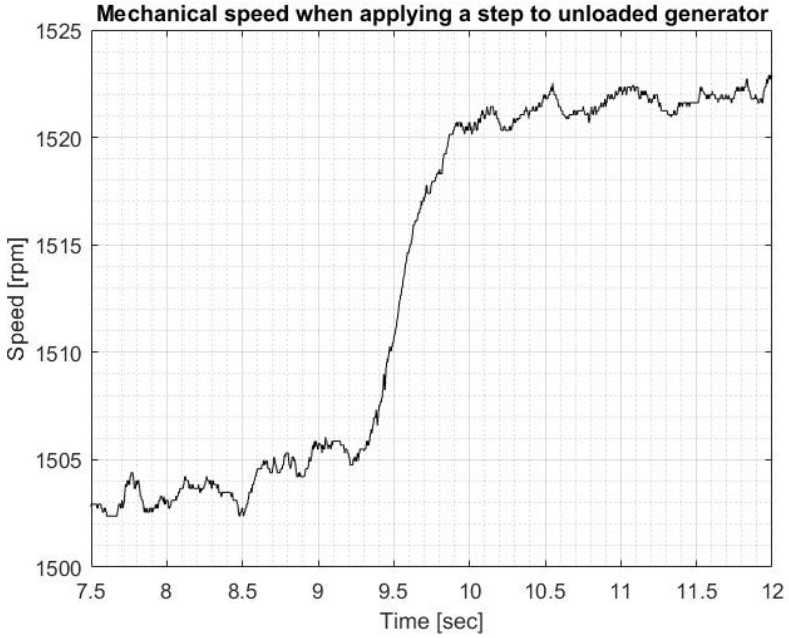

Figure 6.24: Speed plot for an unloaded generator and prime mover.

found in data sheets from Terco [43].

6.6.2 Moment of Inertia With Rated Load

Figure 6.26 is the mechanical torque recorded during the step of 20 rpm, with an active load of 1050 W. The speed- and torque-curves are used to find the parameters needed to calculate the mechanical constants with load.

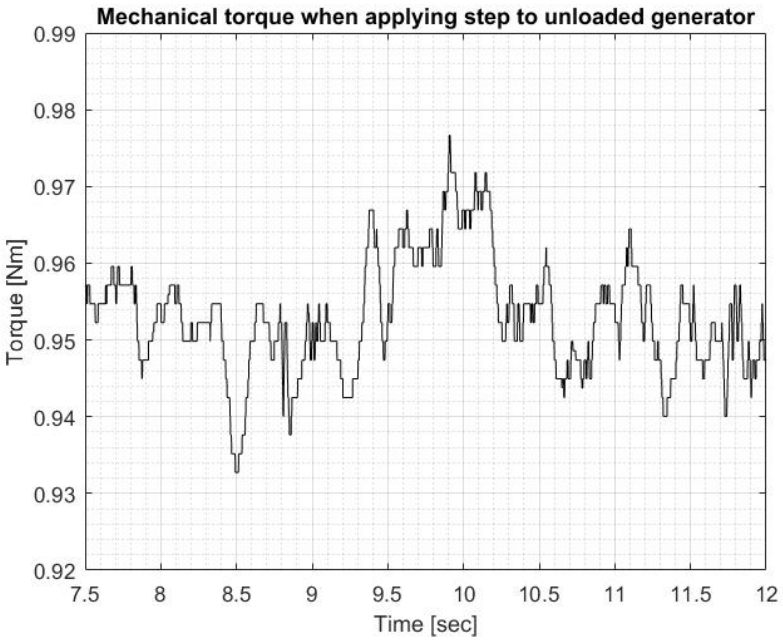

Figure 6.25: Torque plot for unloaded generator and prime mover

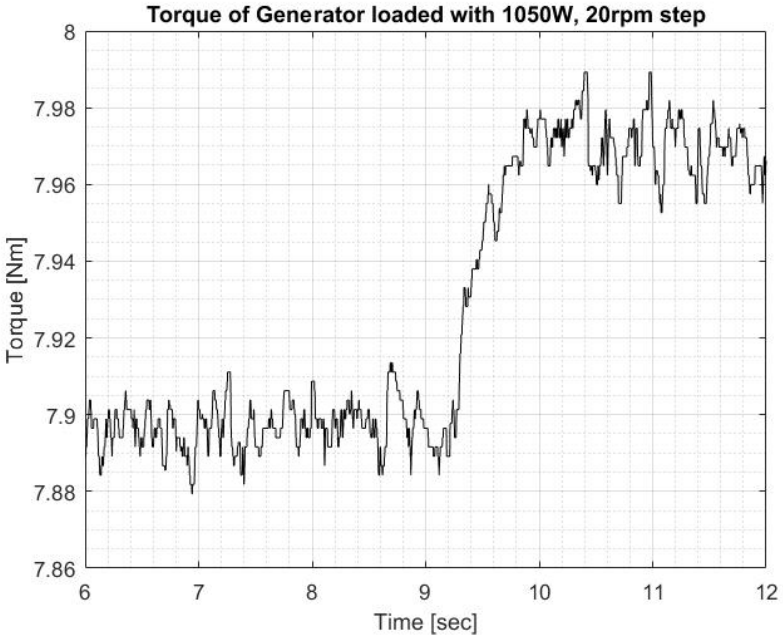

Figure 6.26: Torque plot for generator with 1050W active load.

$$T_{mean.upper} = 7.96\,[Nm] \tag{6.40}$$

$$T_{mean.lower} = 7.89\,[Nm] \tag{6.41}$$

$$\omega_{mean.upper} = 1523\,[rpm] \tag{6.42}$$

$$\omega_{mean.lower} = 1503\,[rpm] \tag{6.43}$$

$$\omega = \frac{n}{60} \times 2\pi \tag{6.44}$$

Where n is speed in revolutions per minute, and ω is in rad/s. The running speed is converted to rad/s using Equation (6.44), yielding max speed 159.5 rad/s and minimum speed 157.4 rad/s. Equation (6.45) is used to find the electromechanical torque the load puts on the synchronous generator.

$$P_e = T_e \times \omega \tag{6.45}$$

Where ω is in radians per second.

$$T_{e.upper} = \frac{1050}{159.5} = 6.58\,[Nm] \tag{6.46}$$

$$T_{e.lower} = \frac{1050}{157.4} = 6.67\,[Nm] \tag{6.47}$$

To calculate the angular acceleration, the time from lower to upper speed was needed. It was found to be 0.86 sec. This must not be confused with the time constant of the system. The interval was found by observing the approximated transfer function for the dynamic response. The angular acceleration is then calculated, then the moment of inertia, and finally, the inertia constant.

$$\dot{\omega} = \frac{159.5 - 157.08}{0.86} = 2.44\,[rad/s^2] \tag{6.48}$$

$$J = \frac{7.96 - 6.58}{2.44} = 0.56\,[kgm^2] \tag{6.49}$$

$$H = \frac{1}{2} \times \frac{0.56 \times (157.08)^2}{1200} = 5.8\,[sec] \tag{6.50}$$

Usually, the inertia constant ranges between 1 and 10 seconds for normal machines. This depends on the size of the machine and which type it is. The prime mover element/turbine affects the constant as well [2, 15].

The mechanical staring time M is calculated in Equation (6.51). In literature both M and T_M is used to denote this time [2, pp. 132].

$$M = 2H = 2 \times 5.8 = 11.6\,[sec] \tag{6.51}$$

The mechanical starting time is the time it takes for rated torque to accelerate the rotor to rated speed from standstill. These constants describe the effect of the kinetic energy stored in the rotor during operation. The mechanical constants are used to model the mechanical part of a power system.

6.7 Measurement in a Laboratory Environment

The work in this thesis has been executed in the Power Electronics laboratory at Western Norway University of Applied Science, campus Kronstad. The objective of the thesis has been solved experimentally in the lab.

6.7.1 Uncertainty in Measurements

Professional measuring equipment were used in the experiments. Table 15 lists the various accuracies of the different instruments and devices used to measure electrical parameters in this thesis. It was not possible to locate any information concern-

Table 15: Accuracy of laboratory instruments

Instrument	Variable	Accuracy
Fluke DP120 Differential Probe	V_{ac}-V_{dc}	±2.5%
Fluke i5s Current Clamp	A_{ac} (10mA-1A)	$\pm 1\% + 5mA$
	A_{ac} (1A-5A)	±1%
Fluke i30s Current Clamp ac/dc	A	±1% of reading ±2%
Fluke 435 Power Quality Analyzer	V_{rms}	±1% of nominal voltage
	A	±0.5%
	Effect	±1%
Hioki DT4282 Multimeter	V_{dc}	±0.025%
	V_{ac}	±0.2%
	R	±0.03%
	I_{dc}	±0.05%
	I_{ac}	±0.6%

ing the accuracy of the Terco MV1054 Digital Torque, Speed and Shaft Power Meter. This component is essential in quantifying experimental measurements, and information regarding its accuracy would be valuable in calculation of the combined uncertainty in measurements.

The devices used holds a very high accuracy. The output variables that were of interest to measure are large compared to the measurement uncertainty, e.g the line-to-line (230 V) voltage compared to the accuracy of the DP120 differential probe ($\pm 5.75 V$). The DP120 has the lowest accuracy of the devices used, and measurement uncertainty could be reduced by using more accurate devices to capture the voltage.

6.7.2 Noise Reduction

Several methods were used to reduce the noise in the system, such as screening, keeping the signal within linear limits etc. Figure 6.27 shows the improvement of the signal, caused by taking these measures.

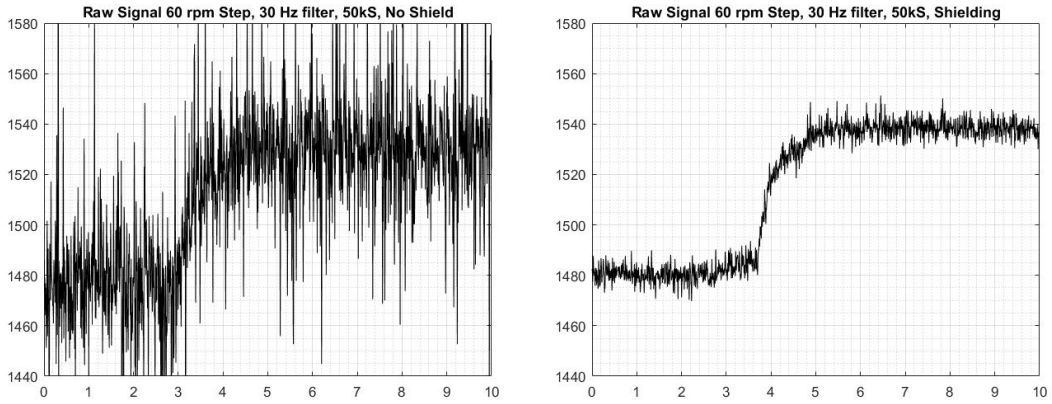

(a) No noise reduction measures taken **(b)** Noise reduction measures employed

Figure 6.27: A 60 rpm step to the drive, 30 Hz filtering in software, 50k sampling rate. The measured signal is the analog 0-10 V output from the Terco MV1054. Essentially showing the impact of shielding components and wires with grounded aluminum foil.

6.7.3 Periodic Noise in Measurements

Sometimes, it was noticed a relatively small periodic disturbance in the signal, once the drive and asynchronous motor was initiated. The disturbance was found in the speed signal from the Terco MV1054 Torque, Speed and Power Meter. The author suspects that this disturbance has an effect on the step response of the

mechanical system. Figure 6.28 shows a typical result from a step response test of

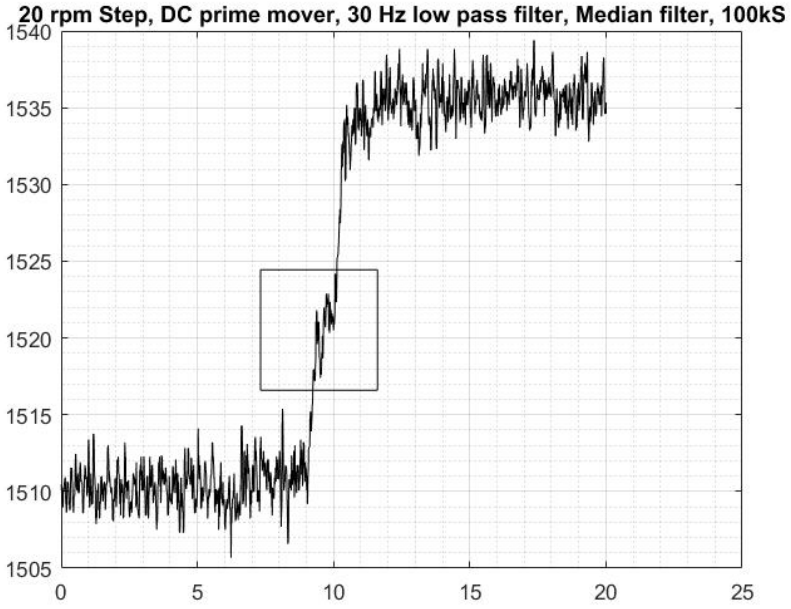

Figure 6.28: Plot showing the periodic disturbance found in most step measurements taken during this thesis. The disturbance is captured in the rectangular box in the plot.

20 rpm. The periodic disturbance is indicated in the rectangular box. The author kept an oscilloscope running, and observed that the disturbance was a reoccurring phenomena, with a period of about 1.5 sec. This means that during a step, the disturbance will affect the response of the system, due to its quick and reoccurring nature.

Tests have been performed with open circuit, rated load, different prime mover machines, and the disturbance was still present in the measurements. The disturbance was only found when speed was measured with the Terco Torque, Speed and Power Meter. It is therefore reasonably to suspect that it is a mechanical disturbance. The phenomenon was not seen when the calculated speed from the VFD was used. A more thorough research will be conducted on this disturbance in a later stage, and will attempt to eliminate it for future studies. It caused some concern at first, but its impact on the response was negligible.

7 Discussion

Load Frequency Control (LFC) is necessary in a modern power system. The stability of frequency and voltage is paramount for optimal system performance. The design of a controller for frequency regulation is therefore a vital part of a complete power system. The LFC implemented in this thesis works with a feedback from the mechanical speed of the rotor. The prime mover is principally represented by an induction machine, as testing with the dc machine did not give satisfying results. The induction machine, being powered by an ABB VFD, was able to satisfactory regulate the system frequency in the event of a load change.

The PID controller was tuned with different rules, which was tested experimentally on the system. The resolution of the VFD was sparse in DTC mode, so the PID parameters was rounded up to the next available figure that could be set on the controller. An understanding of stability limits is important for system operators. Several control system techniques can be used to check stability. Theoretically, stability limits was established. When testing commenced, it showed that it was possible to extend these limits without sacrificing stability.

The tuning limits for the PID did result in stability of the system. The machine operated with synchronous speed, and when additional load was applied to the system, the frequency did not deviate beyond limits defined in standards and by legislation. The LFC designed agrees with the limits presented earlier in this thesis. The controller could be refined to limit the frequency deviation even more, if needed. A lot of time was invested in being acquainted with the ABB ACS 880 VFD. Due to time limitations it was not possible to introduce several controllers. However, the VFD did perform in a satisfactory manner.

Initially, a more extensive work was planned with the dc machine, which is more suited to speed control than other machines. However, some challenges was experienced with the Terco MV2658 PWM DC Control Module that controls the speed of the dc machine. The armature current supplied to the dc machine controls the speed. The MV2658 has a current limit of 7.5 A; the dc machine required a higher current should it be able to sustain synchronous speed when the generator was loaded with rated load. The MV2658 has an analog 0-10 V input for regulating the

duty cycle of the armature current, i.e. the dc machine speed. It was intended to implement the LFC by sending a signal to this port. Experiments showed that 10.6 V was needed to drive an unloaded generator in synchronous speed. When addressing this problem towards the manufacturer, it was concluded that this is a malfunction that will be corrected. The dc machine was used to perform the OCC and SSC tests, with adequate results.

The successful implementation of the LFC makes it possible to conduct further studies in power system stability; a complex and important field of Electric Power engineering. The work in this thesis shows that it is possible to control the active power balance with a VFD. Further work can be invested in optimizing the PID utilized in this thesis. Future work could also involve the design and implication of other control systems. Also, the system with the LFC could be extended with an AVR to model a complete power system; which could be the basis for interesting power system stability case studies.

8 Conclusion

The objective of this thesis was to implement a Load Frequency Control system with a synchronous generator, and conduct experiments to verify frequency stability.

The work started by examining the mechanical system of a synchronous generator, and design a control system to maintain synchronous speed in the event of a disturbance or additional loading. The dynamic response of a power system is affected by multiple parameters. The work in this thesis was conducted on a single-machine case, which is a good way of highlighting the fundamentals of synchronous generator modeling and control.

The work was conducted on a new synchronous generator and dc machine (prime mover), which was acquired and ready to test by the start of March 2017. Delays in delivery from the manufacturer prevented the testing from commencing earlier. It was soon discovered that some of the control devices was not designed for the objective in this thesis. Therefore, an induction machine with an ABB 880 VFD was supplemented into the machine rig shortly after.

The electric parameters of the synchronous generator has been determined through the use of the open-circuit characteristic and the sustained short-circuit test. The slip test has also been executed, and this experiment yielded answers that supported the previous tests. The Potier test was applied in order to find the stator leakage reactance. Due to several weaknesses with the Potier-test, it was not possible to locate the exact stator leakage reactance.

It has been proven that the transfer function of a dynamic system can be found by reviewing the step response. Different step responses have been applied to different parts of the system, resulting in several dynamic models. Important system parameters have been located, such as the delay and time constant. The approximations of the dynamic responses were made for both the prime mover element, and the prime mover and synchronous generator with load. Both approximations were used to determine several PID settings, and these settings were tested with each system.

Mechanical constants for the synchronous generator and induction machine have been established, for rated load and open-circuit. The combination of measured mechanical torque and calculated electromechanical torque were used to derive the moment of inertia. This then led to the inertia constant, and the mechanical starting time. The moment of inertia found is in compliance with values found in data sheets for the machines.

The Load Frequency Control was successfully implemented into the system, to regulate the speed of the generator. The controller utilized the built-in PID controller of the ABB VFD. Restraints on resolution for the VFD PID limited the span of settings the author could manipulate. However, testing revealed very nice results. Further, it was possible to test different tunings in combination with steps in load and running speed. Also, it was possible to maintain synchronous speed when the synchronous generator experienced a change in load. Different responses to additional loading was collected, and the setting which rapidly brought the frequency back to rated value was preferred. This setting also saw least frequency deviation. A stability analysis was performed on the combined system. Stability margins was discovered. The critical gains of the system has been simulated in Matlab.

Through design and implementation of a control, the LFC successfully maintained the system frequency. The author has gained a deeper insight in control system engineering, and the monitoring and regulation of active power from a generator. The controller implemented worked adequate, and can be refined in future studies. The methods used to gather parameters in this thesis proved to yield adequate results, and can be utilized in future LFC models.

References

[1] P. Kundur, J. Paserba, V. Ajjarapu, G. Andersson, A. Bose, C. Canizares, N. Hatziargyriou, D. Hill, A. Stankovic, C. Taylor, T. V. Cutsem, and V. Vittal, "Definition and classification of power system stability ieee/cigre joint task force on stability terms and definitions," *IEEE Transactions on Power Systems*, vol. 19, pp. 1387–1401, Aug 2004.

[2] P. Kundur, *Power System Stability and Control Second Edition.* McGraw Hill, Inc., 1994.

[3] E. N. of Transmission System Operators for Electricity, ""system operation agreement; regarding operation of the interconnected nordic power system"," June 2006.

[4] A. K. H. Markiewicz, ""voltage disturbances standard en50160; voltage characteristics in public distribution systems"," *Power Quality Application Guide*, July 2004.

[5] J. Bermingham, "Benjamin franklin's kite experiment and other electrical discoveries," *Electrical Engineering*, vol. 71, pp. 47–49, Jan 1952.

[6] J. E. Brittain, "Electrical engineering hall of fame: Nikola tesla," *Proceedings of the IEEE*, vol. 93, pp. 1057–1059, May 2005.

[7] N. Tesla, "A new system of alternate current motors and transformers," *Transactions of the American Institute of Electrical Engineers*, vol. V, pp. 308–327, July 1888.

[8] W. E. Mitchell, "Interconnection of power systems in the southeastern states," *Transactions of the American Institute of Electrical Engineers*, vol. XLIII, pp. 1238–1248, Jan 1924.

[9] T. J. Sørås, "Market integration and volatility in the nordic energy exchange," Master's thesis, University of Stavanger, Norway, 2016.

[10] J. Machowski, J. W. Bialek, and J. R. Bumby, *Power System Dynamics: Stability and Control Second Edition.* John Wiley and Sons, Inc., 2012.

[11] ""ieee draft guide for test procedures for synchronous machines part i - acceptance and performance testing –part ii - test procedures and parameter determination for dynamic analysis"," *IEEE Unapproved Draft Std P115/D3, Aug 2009*, 2009.

[12] "Ieee recommended practice for excitation system models for power system stability studies," *IEEE Std 421.5-2016 (Revision of IEEE Std 421.5-2005)*, pp. 1–207, Aug 2016.

[13] "Ieee guide for synchronous generator modeling practices and applications in power system stability analyses," *IEEE Std 1110-2002 (Revision of IEEE Std 1110-1991)*, pp. 01–72, 2003.

[14] S. D. Umans, *Fitzgerald and Kingsley's Electric Machinery seventh edition.* McGraw-Hill International, 2014.

[15] A. R. Bergen and V. Vittal, *Power Systems Analysis second edition.* Prentice Hall Inc, 2000.

[16] N. Jaleeli, L. S. VanSlyck, D. N. Ewart, L. H. Fink, and A. G. Hoffmann, "Understanding automatic generation control," *IEEE Transactions on Power Systems*, vol. 7, pp. 1106–1122, Aug 1992.

[17] F. P. de Mello and J. R. Ribeiro, "Derivation of synchronous machine parameters from tests," *IEEE Transactions on Power Apparatus and Systems*, vol. 96, pp. 1211–1218, July 1977.

[18] J. C. P. Suni, E. Ruppert, and F. Fajoni, "A guide for synchronous generator parameters determination using dynamic simulations based on ieee standards," in *The XIX International Conference on Electrical Machines - ICEM 2010*, pp. 1–6, Sept 2010.

[19] R. H. Park and B. L. Robertson, "The reactances of synchronous machines," *Transactions of the American Institute of Electrical Engineers*, vol. 47, pp. 514–535, April 1928.

[20] J. G. Ziegler and N. B.Nichols, "Optimum settings for automatic controllers," in *The American Society of Mechanical Engineers*, pp. 759–765, December 1942.

[21] N. S. Nise, *Control System Engineering sixth edition.* John Wiley and Sons, Inc., 2011.

[22] R. H. Park, "Two-reaction theory of synchronous machines generalized method of analysis-part i," *Transactions of the American Institute of Electrical Engineers*, vol. 48, pp. 716–727, July 1929.

[23] R. H. Park, "Two-reaction theory of synchronous machines-ii," *Transactions of the American Institute of Electrical Engineers*, vol. 52, pp. 352–354, June 1933.

[24] J. A. Short, D. G. Infield, and L. L. Freris, "Stabilization of grid frequency through dynamic demand control," *IEEE Transactions on Power Systems*, vol. 22, pp. 1284–1293, Aug 2007.

[25] A. Bose and I. Atiyyah, "Regulation error in load frequency control," *IEEE Transactions on Power Apparatus and Systems*, vol. PAS-99, pp. 650–657, March 1980.

[26] H. Saadat, *Power Systems Analysis third edition.* PSA Publishing, 2010.

[27] S. H. Wright, "Determination of synchronous machine constants by test reactances, resistances, and time constants," *Transactions of the American Institute of Electrical Engineers*, vol. 50, pp. 1331–1350, Dec 1931.

[28] J. C. Peqqueña, E. Ruppert, and M. T. Mendoza, "On the synchronous generator parameters determination using dynamic simulations based on ieee standards," in *2010 IEEE International Conference on Industrial Technology*, pp. 386–391, March 2010.

[29] S. K. Goswami, "Synchronous-machine sudden 3-phase short-circuit. analysis by norton's, constant-flux-linkage and thÃ©venin's theorems," *Electrical Engineers, Proceedings of the Institution of*, vol. 118, pp. 1459–1466, October 1971.

[30] A. M. El-Serafi and J. Wu, "A new method for determining the armature leakage reactance of synchronous machines," *IEEE Transactions on Energy Conversion*, vol. 6, pp. 120–125, Mar 1991.

[31] Z. D. Grève, M. Delhaye, G. Lossa, and F. Vallée, "Contribution to the determination of the stator leakage reactance of synchronous generators," in *2013 IEEE International Conference on Industrial Technology (ICIT)*, pp. 284–289, Feb 2013.

[32] L. A. March and S. B. Crary, "Armature leakage reactance of synchronous machines," *Electrical Engineering*, vol. 54, pp. 378–381, April 1935.

[33] J. P. Bentley, *Principles of Measurement Systems Fourth Edition.* Person Education Limited, 2005.

[34] I. Kamwa, M. Pilote, P. Viarouge, B. Mpanda-Mabwe, M. Crappe, and R. Mahfoudi, "Experience with computer-aided graphical analysis of sudden-short-circuit oscillograms of large synchronous machines," *IEEE Transactions on Energy Conversion*, vol. 10, pp. 407–414, Sep 1995.

[35] I. Kamwa, M. Pilote, H. Carle, P. Viarouge, B. Mpanda-Mabwe, and M. Crappe, "Computer software to automate the graphical analysis of sudden-short-circuit oscillograms of large synchronous machines," *IEEE Transactions on Energy Conversion*, vol. 10, pp. 399–406, Sep 1995.

[36] L. Halbo, *Kvalitetsstyring og Måleteknikk i laboratorium, produksjon og tjenestevirksomhet.* Gyldendal Forlag, 2010.

[37] N. S. Narkhede, A. B. Kadu, and S. Y. Sondkar, “Labview based system for pid tuning and implementation for a flow control loop,” in *2016 International Conference on Advanced Communication Control and Computing Technologies (ICACCCT)*, pp. 436–442, May 2016.

[38] J. Skaare, *Regulering av turbiner i vannkraftverk - En litteratur studie*. PhD thesis, Norges miljø- og biovitenskapelige universitet, 2014.

[39] R. McElveen, J. Korkeakoski, and J. Malinowski, “Electrical and mechanical differences between nema/ieee and iec ac low voltage random wound induction motors,” in *2012 Petroleum and Chemical Industry Conference (PCIC)*, pp. 1–10, Sept 2012.

[40] G. C. Goodwin, S. F. Graebe, and M. E. Salgado, *Control System Design*. Prentice Hall, 2001.

[41] Terco, *Digital Torque, Speed, Shaft Power Meter*, 4 2017.

[42] O. og energidepartementet, “"forskrift om leveringskvalitet i kraftsystemet",” June 2004.

[43] Terco, *Electric Machine Laboratory*, 4 2017.

A Laboratory Instruments

Table over instruments and devices used during the experimental work done in this thesis.

Table 16: Instruments and devices

Instrument	Manufacturer	Quantity
Digital oscilloscope	Picoscope 4824	1
Power Analyzer	Fluke 435 Power Quality Analyzer	1
DC source 0-60VDC		2
Digital Multimeter	Hioki	2
Differential voltage probes	Fluke DP120	5
Current clamps	Fluke i5s	4
Synchronous machine	Terco MV1027-235	1
DC machine	Terco 1028-225	1
Digital Torque, Speed and Shaft Power Meter	Terco MV1054	1
PWM DC Control Module	Terco MV2658	1
Asynchronous machine	Terco MV1009	1
Load Reactor	Asea	1
Load Reactor	Terco MV1101	1
Load Resistor	Terco MV1100	1
Variable Frequency Drive	ABB ACS880-01	1
AC/DC Power Supply	Langlois Compak40	1

B DC Machines

The dc machine is a versatile machine, that is suited to a wide range of applications. Using shunt-, series, and separately excited field windings they can be designed to a number of different volt-ampere or speed-torque characteristics [14, pp. 403]. The dc machine can easily be controlled, and has been used in applications requiring a wide range of motor speeds or precise control. In recent years the induction motor with VFD has replaced the dc motor, but the simplicity of the dc machine sees its continued use in various applications.

The stator has salient poles, and is excited by one or more field windings. The flux distribution created by the field windings is symmetric along the center line of the field poles, and is dubbed the direct axis. The armature terminals are found on the

rotor, and generate an ac voltage. A rotating commutator and stationary brushes convert the ac armature voltage at its terminals into a dc voltage. Together, the commutator and brushes form a mechanical rectifier [14, pp. 403]. The brushes are located midways between the field poles, so that commutation occurs when the coil sides are in the neutral zone. When the dc machine is operating as a generator,

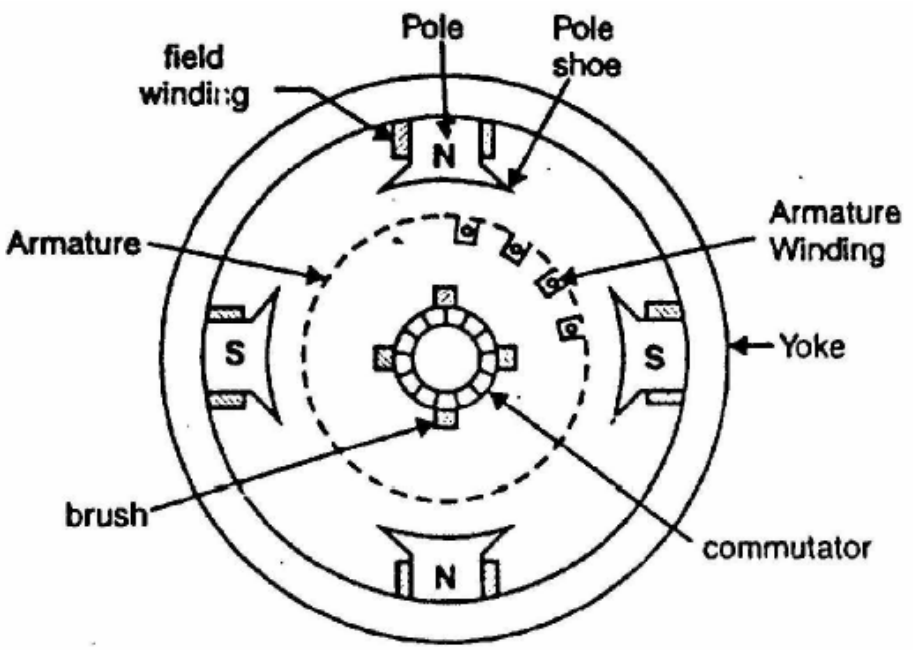

Figure B.1: Crossection of a dc machine

the electromagnetic torque opposites rotation. When the machine is working as a motor, the torque acts in the directing of the rotation. The torque of a dc machine is the result of an interaction between two different flux distributions within the machine. The commutators is fixed, so when direct current is flowing through the brushes, it creates a magnetic flux distribution which is fixed in space. This distribution has an axis which is typically perpendicular to the field flux [14, pp. 202].

The mechanical torque of a machine is expressed in terms of the direct-axis air gap flux per pole and the space-fundamental component of the armature mmf-wave [14, pp. 404].

$$T_{mech} = \left(\frac{poles C_a}{2\pi m} \right) \Phi_d i_a = K_a \Phi_d i_a \tag{B.1}$$

Where i_a is the current in the external armature circuit, C_a is the total number of conductors in the armature winding and m is the number of parallel paths through the winding. From Equation (B.1) it is seen that K_a is a constant that is determined by the design of the winding.

The most important limiting factor for dc machines is the ability to transfer the necessary dc armature current through the contacts. Satisfactory operation demands that armature current is delivered without excessive sparking at the brushes. Sparking causes local losses, and is partly responsible for heating of the machine [14, pp 442].

C Induction Machines

Induction machines, also called asynchronous machine, have roughly the same build-up as synchronous machines. The magnetic forces act in a similar manner for both machines, the difference between them is how we obtain the magnetizing energy. Induction machines drain reactive power from the grid to maintain their magnetic field, while in synchronous machines direct current is supplied to the field windings.

Thus, a slip from the synchronous speed, which is determined by the number of poles in the machine, will be noticed. Induction machines produce torque only when the rotor speed differs from synchronous speed [14, pp. 199]. This happens because current are induced in the shorted rotor windings as the rotor is slipping past the synchronously-rotating armature flux wave. Often, the shorted rotor is referred to as a squirrel cage.

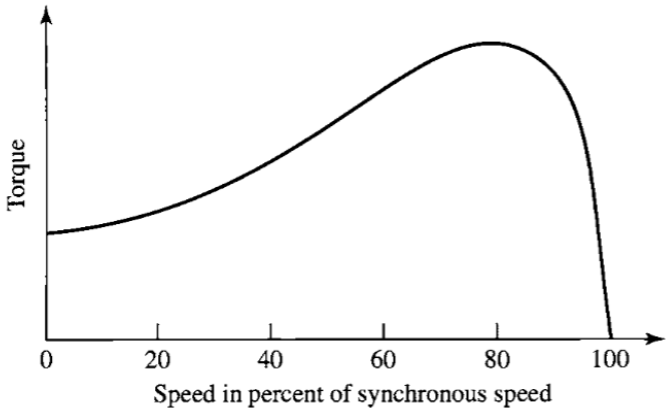

Figure C.1: A typical graph of the motor speed-torque characteristic for asynchronous machines [14].

Induction machines is commonly used as a motor, its use as a generator is limited due to the reactive power needed to magnetize the machine. Due to its simple design and low cost, the asynchronous machine is one of the most popular machines used in commercial systems. As a motor there are few competitors. If the induction machine is used to produce electrical energy, it sees most us as a generator in wind mills.